Available online at www.sciencedirect.com
SCIENCE DIRECT®
ELSEVIER
International Journal of Solids and Structures 43 (2006) 5421–5448
INTERNATIONAL JOURNAL OF SOLIDS and STRUCTURES
www.elsevier.com/locate/ijsolstr

Extended finite element method in plasticity forming of powder compaction with contact friction

A.R. Khoei *, A. Shamloo, A.R. Azami

Department of Civil Engineering, Sharif University of Technology, P.O. Box 11365-9313, Tehran, Iran

Received 27 April 2005
Available online 18 January 2006

Abstract

In this paper, a new computational technique is presented based on the eXtended Finite Element Method (X-FEM) in pressure-sensitive plasticity of powder compaction considering frictional contact. In X-FEM, the need for mesh adaption to discontinuity interface is neglected and the process is accomplished by partitioning the domain with some triangular sub-elements whose Gauss points are used for integration of the domain of the elements. The technique is applied by employing additional functions, which are added to approximate the displacement field of the elements located on the interface. The double-surface cap plasticity model is employed within the X-FEM framework in numerical simulation of powder material. The plasticity model includes a failure surface and an elliptical cap, which closes the open space between the failure surface and hydrostatic axis. The moving cap expands in the stress space according to a specified hardening rule. The frictional behavior of contact between two bodies is modeled by using the X-FEM technique and applying the Heaviside enrichment function. The application of X-FEM technique in simulation of pressure-sensitive material is presented in an incremental manner and the role of sub-elements in simulation of contact treatment is demonstrated. Finally, several numerical examples are analyzed with special reference to plasticity forming of powder compaction.

Keywords: Extended FEM; Partition of unity; Cap plasticity; Contact friction; Powder compaction

1. Introduction

In powder compaction simulation, the note for mesh adaption in different stages of process is of great importance. The need for mesh conforming to the shape of the boundary of mould must be preserved at each stage of compaction. The requirement of mesh adaptation in this process may consume high expenses of capacity and time in computer simulation. Thus, it is necessary to perform an innovative procedure to remove the limitation of the mesh conforming to the boundary conditions. One of the methods that has been successfully employed in modeling cracks and inhomogeneities is the eXtended Finite Element Method (X-FEM), in which its application is widely spread in the problems with different boundary conditions. In X-FEM, the need

* Corresponding author. Tel.: +98 21 6005818; fax: +98 21 6014828.
E-mail address: arkhoei@sharif.edu (A.R. Khoei).

0020-7683/$ - see front matter © 2005 Elsevier Ltd. All rights reserved.
doi:10.1016/j.ijsolstr.2005.11.008

for remeshing and mesh adaption can be neglected if discontinuity or crack propagation happens. In this technique, the standard displacement based approximation is enriched by incorporating discontinuous fields through a partition of unity method (Melenk and Babuska, 1996). Mesh adaption process is therefore substituted by partitioning the domain with some triangular sub-elements whose Gauss points are used for integration of the domain of elements. The important advantage of the method is that the number of degrees of freedom remains constant and thus, we do not need to solve a greater equation. In this case, additional functions are used to enrich the discontinuous displacement fields of the domain, which compensate for this discontinuity.

The most application of X-FEM technique has been reported in modeling crack growth and crack propagation. The method was first developed by Dolbow (1999), Belytschko and Black (1999) and Moes et al. (1999) to model cracks, voids and inhomogeneities. They proposed appropriate additional terms in finite element approximation based on the partition of unity method (Melenk and Babuska, 1996). This allows for the entire crack geometry to be modeled independently of the mesh, and completely avoids the need to remesh as the crack grows. A methodology that constructs the enriched approximation based on the interaction of the discontinuous geometric features with the mesh was developed by Daux et al. (2000) in modeling crack discontinuities. The implementation of the X-FEM into three-dimensional crack modeling was presented by Sukumar et al. (2000) using the notion of partition of unity. Belytschko et al. (2001) developed a technique in modeling arbitrary discontinuities in finite elements. In this method, the discontinuous approximation was constructed in terms of a signed distance functions and the level sets were used to update the position of the discontinuities. Dolbow et al. (2001) proposed special treatments in numerical simulation of crack growth, in which the frictional contact was modeled in the framework of X-FEM technique and an iterative procedure, called 'LATIN method' was applied in the analysis of contact faces of crack. In this method, the nonlinear behavior of contact was incorporated into the linear global equations by an iterative scheme to resolve the nonlinear boundary value problem. The combination of this method with X-FEM was enhanced the solution procedure of contact analysis, efficiently. An algorithm which couples the level set method with the extended finite element method was proposed by Stolarska et al. (2001). They applied a discontinuous function based on the Heaviside step function in modeling two-dimensional linear elastic crack-tip displacement fields.

An enriched finite element method for the multi-dimensional Stefan problems was presented by Chessa et al. (2002). In this method, the standard finite element basis was enriched with a discontinuity in the derivative of the temperature normal to the interface, in which the phase interface was evolved without remeshing, or the use of artificial heat capacity techniques. A hybrid numerical method was proposed by Ji et al. (2002) for modeling the evolution of sharp phase interfaces on fixed grids, with reference to solidification problems. They employed the enrichment strategies of X-FEM to represent the jump in the temperature gradient that governs the velocity of the phase boundary. Moes and Belytschko (2002) proposed the X-FEM technique in modeling growth of cohesive cracks by eliminating the evaluation of stress intensity factors at the tip of the cohesive zones. The method was applied by Patzák and Jirásek (2003) for the computational resolution of highly localized strains in narrow damage process zones of brittle materials. A methodology for modeling crack discontinuities was presented by Sukumar and Prevost (2003) with implementation of X-FEM in isotropic and biomaterial media. The technique was implemented into three-dimensional fatigue crack propagation simulation of multiple coplanar cracks by Sukumar et al. (2003) and Chopp and Sukumar (2003). They combined the extended finite element method to the fast marching method using the partition of unity method to model the entire crack geometry, including one or more cracks, by a single signed distance (level set) function. The X-FEM is applied in two-phase flow problems by Chessa and Belytschko (2003), in which the interface can move arbitrarily through the mesh without remeshing and the discontinuity in the velocity gradient at the interface is modeled by a local partition of unity. An enriched finite element method with arbitrary discontinuities in space–time was presented by Chessa and Belytschko (2004). They modeled discontinuities by the X-FEM with a local partition of unity enrichment to introduce discontinuities along a moving hyper-surface.

The application of X-FEM in plasticity behavior of material is a pristine field. The aim of present study is to implement the method in pressure-sensitive plasticity material, such as compaction forming of powder, as the necessity of remeshing can be observed in most conditions. Powder forming considers the methods of

producing commercial products from metallic powders by pressure. The compaction of powders shows three complex densification mechanisms. Firstly, at low pressure, particle sliding occurs leading to particle rearrangement. The second stage involves both elastic and plastic deformation of the particles via their contact areas leading to geometric hardening (i.e., plastic deformation and void closure). Lastly, at very high pressure, the flow resistance of the material increases rapidly due to material strain hardening. In order to perform such complex mechanisms, the process of compaction must be drawn into a mathematical formulation with the knowledge of material behavior. Constitutive modeling of powder is therefore one of the main ingredients of successful quantitative solution possibilities, which can reproduce powder material behavior under complicated loading conditions.

A number of constitutive models for the cold compaction of metal powders have been proposed during last three decades, including: microscopic models (Fleck et al., 1992, 1995; Ransing et al., 2000; McMeeking et al., 2001), flow formulations (Lewis et al., 1993) and solid mechanics models (Brown and Weber, 1988; Chenot et al., 1990; Brekelmans et al., 1991; Haggblad and Oldenburg, 1994; Lewis and Khoei, 1998). A visco-plastic model was developed by Storakers et al. (1999) for the densification of spherical powders. Redanz (2001) proposed two different rate-independent elasto-plastic models based on the combined Fleck et al. (1992)–Gurson (1977) model and a modified version of the Fleck (1995) model to simulate the cup-shaped powder component. The mixed yield functions were employed by Kim and Cho (2001) in terms of the volume fractions and the fraction of contact of soft and hard powders. Cedergren et al. (2002) employed two different porous visco-plastic material models based on the combined Fleck et al. (1992)–Gurson (1977) model and the Shima and Oyane (1976) model. A density-dependent endochronic theory was developed by Khoei et al. (2003) and Khoei and Bakhshiani (2004) based on coupling between deviatoric and hydrostatic behavior in finite strain plasticity to simulate the compaction process of powder material.

The experimental results of Watson and Wert (1993) and Brown and Abou-Chedid (1994) demonstrated that the constitutive modeling of geological and frictional materials can be utilized to construct the suitable phenomenological constitutive models which capture the major features of the response of initially loose powders to the complex deformation processing histories encountered in the manufacture of engineering components by powder metallurgy techniques. In particular, they suggested that a 'two-mechanism-model', such as Drucker–Prager or Mohr–Coulomb and elliptical cap models, which are widely used for geological materials and exhibit pressure dependent behavior can be useful for modeling the response of powder materials. These models consist of two yield surfaces; a 'distortion surface' and a 'consolidation' or 'cap' surface, which has an elliptical shape. The distortion surface controls the ultimate shear strength of material and the cap surface captures the hardening behavior of material under compression.

The cap plasticity model used in the modeling of geological and frictional materials, is therefore employed to capture the major features of the response of initially loose metal powders to complex deformation histories which are encountered in the manufacture of engineering components by powder metallurgy techniques. The cone-cap model based on a density-dependent Drucker–Prager yield surface and a non-centered ellipse is developed by Aydin et al. (1996), Khoei and Lewis (1998, 1999), Brandt and Nilsson (1999), Gu et al. (2001) and Lewis and Khoei (2001). In this study, a cone-cap density-dependent plasticity model is developed based on a combination of a convex yield surface consisting of a failure envelope and a hardening elliptical cap for nonlinear behavior of powder materials in the concept of the generalized plasticity formulation. A general algorithm for the cap plasticity from the viewpoint of efficient numerical modeling is presented. The cap plasticity together with frictional contact algorithm are performed within the framework of extended finite element method, in order to predict the non-uniform relative density distribution during powder-die pressing. The discontinuity between tool and powder is modeled using the enrichment functions, whose geometry is not dependent on the topology of the mesh. The Heaviside enrichment function is implemented in simulation of powder-die contact surface and the level set function is used for enriching the discontinuities of material properties.

The plan of the paper is as follows: in Section 2, an overview of the extended finite element method is presented with an introduction to the partition of unity method and enrichment of displacement field. In Section 3, the governing equations of nonlinear elasto-plasticity is extracted in the concept of X-FEM. The computational algorithm of frictional contact in X-FEM using an iterative procedure of LATIN method is presented in Section 4. In Section 5, the double-surface cap plasticity is developed for description of powder behavior. The

derivation of constitutive elasto-plastic matrix and its components, and parameter determination of double-surface plasticity are demonstrated in this section. In Section 6, numerical simulation of several complicated die geometries are presented. Finally, some concluding remarks are given in Section 7.

2. The extended finite element method

The enriched finite element methods are powerful and accurate approaches to model discontinuities without considering their geometries. In these methods, the discontinuities are not considered in mesh generation operation and special functions which depend on the nature of discontinuity are included into finite element approximation. The extended finite element method is one of the most recent approaches, which has been extensively employed in numerical modeling of crack growth. The aim of this method is to simulate the discontinuity with minimum enrichment. In X-FEM, the external boundaries are only consideration in mesh generation operation and internal boundaries, such as cracks, voids, contact surfaces, etc., have no effect on mesh configurations. This method has proper applications in problems with moving discontinuities, such as punching, phase changing, crack propagation, and shear banding.

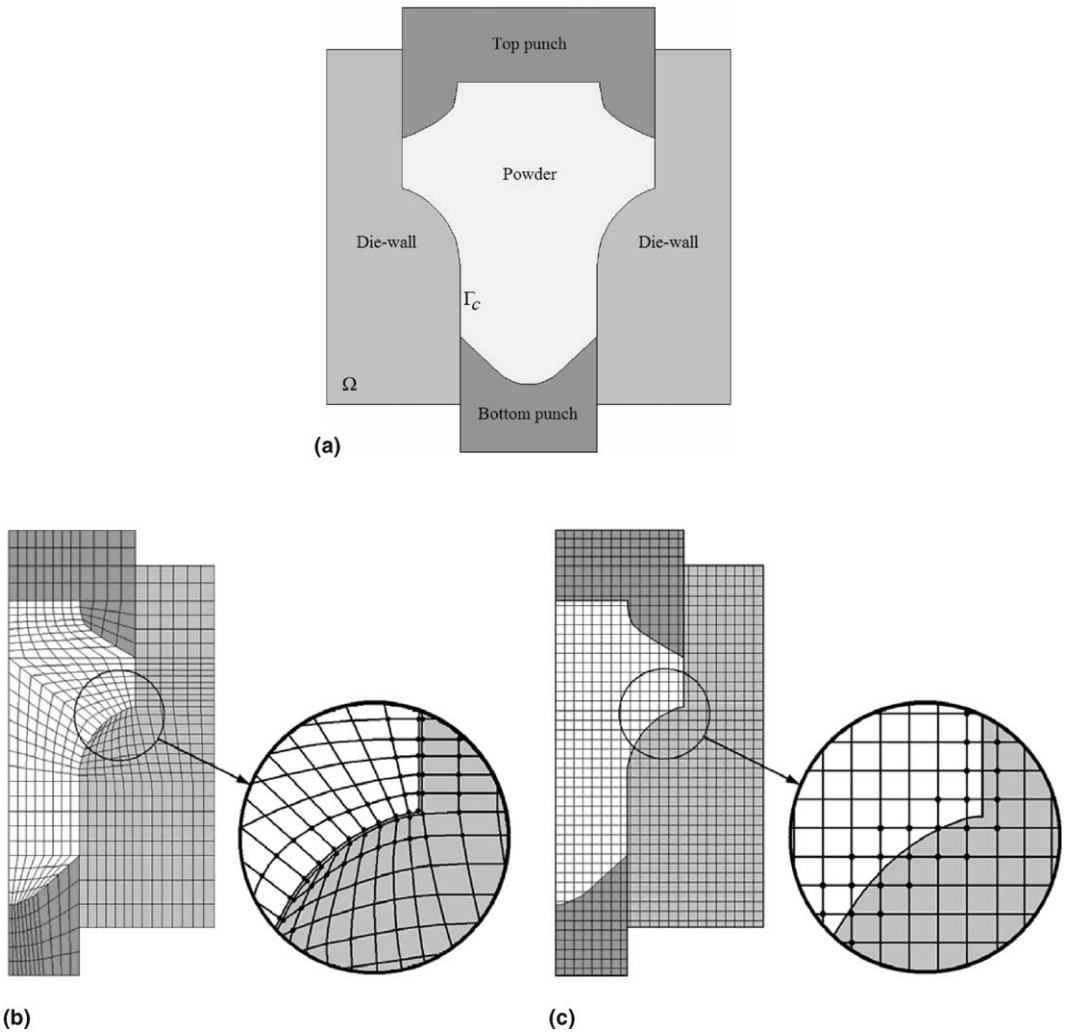

Fig. 1. Modeling of contact surface between powder and die in powder compaction simulation: (a) an axisymmetric shaped tip component, (b) the FE mesh which conforms to the geometry of contact together with employed contact elements and (c) a uniform mesh in which the circled nodes have additional degrees of freedom and enrichment functions.

In order to introduce the concept of discontinuous enrichment, consider that Γ_c be a discontinuity surface between the tool and powder in domain Ω, as shown in Fig. 1(a). We are interested in the construction of a finite element approximation to the field $\boldsymbol{u} \in \Omega$ which can be discontinuous along contact surface Γ_c. The traditional approach is to generate the mesh to conform to the line of contact surface as shown in Fig. 1(b), in which the element edges align with Γ_c, and implement the contact elements in the line of discontinuity surface (Khoei and Lewis, 1998). While this strategy certainly creates a discontinuity in the approximation, it is cumbersome if the line Γ_c evolves in time, or if several different configurations for Γ_c are to be considered (Khoei and Lewis, 1999). In this study, we intend to model the discontinuity along contact surface Γ_c with extrinsic enrichment, in which the uniform mesh of Fig. 1(c) is capable of modeling the contact surface in $\boldsymbol{u}$ when the circled nodes are enriched with functions which are discontinuous across Γ_c.

The standard FE approximation can be enriched with additional functions by using the notion of partition of unity (Melenk and Babuska, 1996). The enriched approximation in modeling of discontinuity Γ_c can be expressed in following form:

$$\mathbf{u}^h(\boldsymbol{x}) = \sum_i N_i(x)\mathbf{u}_i + \sum_j N_j(\boldsymbol{x})\psi(x)\mathbf{a}_j \quad \text{for } n_i \in \mathbf{n}_T \text{ and } n_j \in \mathbf{n}_e \tag{1}$$

The first term of above equation denotes the classical finite element approximation and the second term indicates the enrichment function considered in X-FEM. In this equation, $\mathbf{u}_i$ is the classical nodal displacement, $\mathbf{a}_j$ the nodal degrees of freedom corresponding to the enrichment functions, $\psi(\boldsymbol{x})$ the enrichment function, and $N(\boldsymbol{x})$ the standard shape function. In Eq. (1), $\mathbf{n}_T$ is the set of all nodal points of domain, and $\mathbf{n}_e$ the set of nodes of elements located on discontinuity, i.e.,

$$\mathbf{n}_e = \{n_j : n_j \in \mathbf{n}_T, \omega_j \cap \Gamma_c \neq 0\} \tag{2}$$

In the above equation, $\omega_j = \text{supp}(n_j)$ is the support of the nodal shape function $N_j(\boldsymbol{x})$, which consists of the union of all elements with n_j as one of its vertices, or in other words the union of elements in which $N_j(\boldsymbol{x})$ is non-zero.

In this method, two approaches are simultaneously applied to the elements located on discontinuity; the *partition of unity method* and the *enrichment of displacement field*. The partition of unity method is used to discretize the intersected elements by partitioning the domain with some triangular sub-elements whose Gauss points are used for integration of the domain of elements (Fig. 2a). The enrichment of displacement field is applied to correct the standard displacement based approximation by incorporating discontinuous fields through a partition of unity method (Fig. 2b). It must be noted that the enrichment varies from node to node and many nodes require no enrichment, which is an application of the partition of unity concept. In X-FEM, the diversity in types of problems requires proposing appropriate enrichment functions. Different techniques may be used for the enrichment function; these functions are related to the type of discontinuity and its influences on the form of solution. These techniques are based on the signed distance function, branch function, Heaviside jump function, level set function, etc.

The *signed distance function* is applicable to crack problem, which is discontinuous across the crack line (Belytschko et al., 2001). The function can be viewed as an enrichment with a windowed step function, where $N(\boldsymbol{x})$ is the window function. The window function localizes the enrichment so that the discrete equations will be sparse. For cracks which are not straight, a mapping is required to align the near-tip discontinuities with the crack edges. In this case, a near-tip function, or *branch function*, can be constructed in terms of the distance function, which enables the discontinuity to be curved or piecewise linear (Dolbow et al., 2001). This function spans the near-tip asymptotic solution for a crack, and gives very good accuracy for these problems. The *level set method* is a numerical scheme developed by Sethian (1996) for tracking the motion of interfaces. In this technique, the interface is represented as the zero level set of a function of one higher dimension. This method, which is used for predicting the geometry of boundaries, is distinguished as a good option for inhomogenous fields and its application in enriching the domains which have discontinuity in strain field is considerable. Recently, the technique of *fast marching method*, which was first introduced by Sethian (1999), was coupled with X-FEM to model crack growth (Sukumar et al., 2003 and Chopp and Sukumar, 2003). The method computes the crossing time map for a monotonically advancing front in an arbitrary number of spatial dimensions.

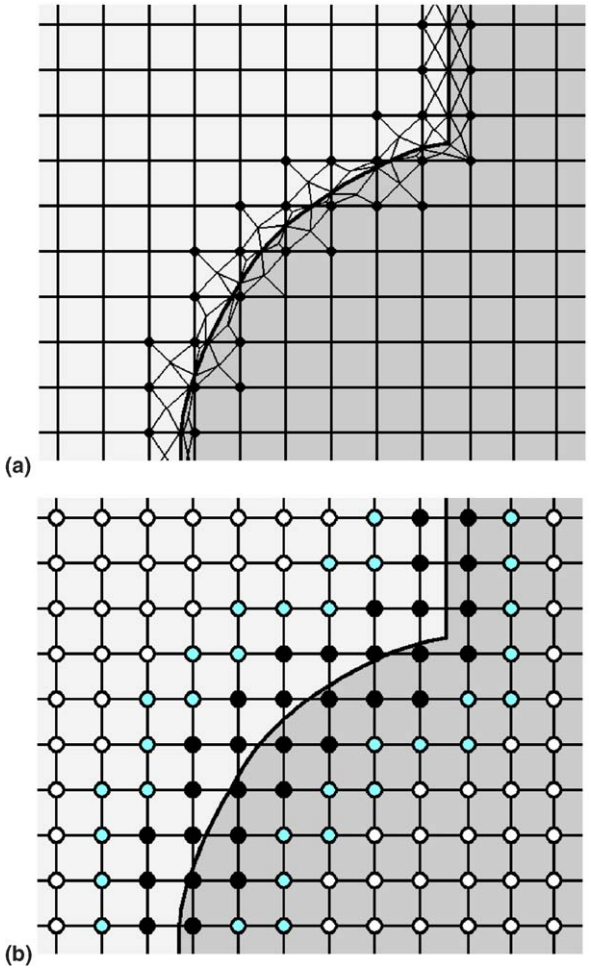

Fig. 2. The extended finite element mesh: (a) the sub-triangles associated with elements cut by contact surface, (b) partition of unity enrichment for elements with the contact surface, (●) fully enriched nodes (set $\mathbf{n}_e$), (○) partially enriched nodes (set $\mathbf{n}_\psi$), and (○) unenriched nodes.

It must be noted that the partition of unity method must be applied together with the enrichment of displacement field to those elements located on the discontinuity surface. The choice of enrichment functions in displacement approximation is dependent on the conditions of problem. If the discontinuity is as a result of different types of material properties, such as powder–punch interface, then the level set function is proposed as an enrichment function—however, if the discontinuity is due to different displacement fields on either sides of the discontinuity, such as contact surface, then the Heaviside function is appropriate. In what follows, the implementation of the level set function in modeling the discontinuity due to different material properties and the Heaviside function in simulation of powder-die contact surface are presented.

In order to model the discontinuity in inhomogeneity due to different material properties of powder and die in two intersected parts, the level set method is used for the elements having discontinuity. The method is a numerical technique for tracking moving interfaces (Sethian, 1996, 1999). A moving interface $\Gamma(t)$ is formulated by the level set function φ, as

$$\Gamma(t) = \{\boldsymbol{x} \in \Re^2 : \varphi(\boldsymbol{x}, t) = 0\} \tag{3}$$

in which the value of level set function is zero on the border. The sign of its value is negative in one side and positive on the other side. The values of level set function present the distance from the border, i.e.,

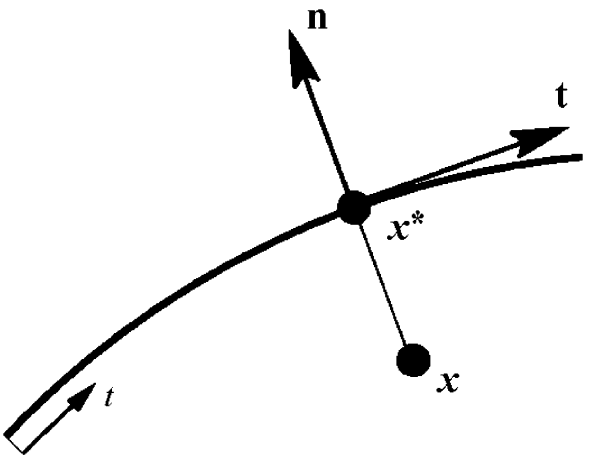

Fig. 3. Illustration of normal and tangential coordinates for a contact surface in the case of jump function $H(\boldsymbol{x}) = -1$; $\boldsymbol{x}^*$ is the closest point to $\boldsymbol{x}$ on the contact surface.

$$\varphi(\boldsymbol{x}) = \min \|\boldsymbol{x} - \boldsymbol{x}^*\| \text{sign}((\boldsymbol{x} - \boldsymbol{x}^*)\mathbf{n}) \tag{4}$$

where $\boldsymbol{x}^*$ is the point on the interface boundary which has the closest distance from the point $\boldsymbol{x}$, and $\mathbf{n}$ is the normal vector to the interface at point $\boldsymbol{x}^*$. These changes in the values of level set make an appropriate behavior for the corrected shape functions. The new degrees of freedom $\mathbf{a}_j$ corresponding to the level set enrichment function are considered in Eq. (1) in order to attribute to the nodes that belong to the set of $\mathbf{n}_e$. The presence of these new degrees of freedom improves the discontinuity due to different types of material properties in two intersected parts of element. In order to improve the numerical computation in X-FEM, it is preferable to have a uniform distribution of shape functions around the boundary of discontinuity. To this goal, a technique for smoothing the values of level set proposed by Sukumar et al. (2000) is applied here by employing the nodes that belong to the elements in the neighbor of discontinuity elements, as shown in Fig. 2(b).

In order to model the discontinuities in displacement fields, the Heaviside enrichment function is implemented in simulation of powder-die contact surface, in which the function $H(\boldsymbol{x})$ takes the value of $+1$ in one side of contact surface, and -1 on the other side, as

$$H(\boldsymbol{x}) = \begin{cases} +1 & \text{if } (\boldsymbol{x} - \boldsymbol{x}^*)\mathbf{n} \geqslant 0 \\ -1 & \text{otherwise} \end{cases} \tag{5}$$

in which the contact surface is considered to be a curve parameterized by the curvilinear coordinate s, as shown in Fig. 3. It must be noted that the Heaviside function is a powerful and reliable tool in enriching the domain with strong discontinuities, such as contact surface.

3. The X-FEM formulation

In this section, the governing equations of nonlinear elasto-plasticity is presented together with the weak form and the discrete system for the X-FEM. Applying the level set enrichment function $\psi(\varphi(\boldsymbol{x}))$ in Eq. (1), the X-FEM displacement approximation can be rewritten as

$$\mathbf{u}(\boldsymbol{x}) = \sum_i N_i(\boldsymbol{x})\mathbf{u}_i + \sum_j N_j(\boldsymbol{x})\psi(\varphi(\boldsymbol{x}))\mathbf{a}_j \quad \text{for } n_i \in \mathbf{n}_T \text{ and } n_j \in \mathbf{n}_e \tag{6}$$

Defining the enrichment function $\psi(\boldsymbol{x})$ based on its nodal values as $\psi(\boldsymbol{x}) = \left|\sum_i N_i(\boldsymbol{x})\psi_i\right|$, Eq. (6) can be rewritten as

$$\mathbf{u}(\boldsymbol{x}) = \sum_i N_i(\boldsymbol{x})\mathbf{u}_i + \sum_j \left(N_j(\boldsymbol{x}) \left| \sum_k N_k(\boldsymbol{x})\psi_k \right| \mathbf{a}_j \right) \quad \text{for } n_i \in \mathbf{n}_T \text{ and } n_j \in \mathbf{n}_e \tag{7}$$

The relationship between strain and displacement can be expressed by taking the derivative of displacement field as

$$\boldsymbol{\varepsilon} = \sum_i \frac{\partial N_i}{\partial \boldsymbol{x}} \mathbf{u}_i + \sum_j \left[\frac{\partial N_j}{\partial \boldsymbol{x}} \left| \sum_k N_k(\boldsymbol{x}) \psi_k \right| + N_j(\boldsymbol{x}) \frac{\partial}{\partial \boldsymbol{x}} \left| \sum_k N_k(\boldsymbol{x}) \psi_k \right| \right] \mathbf{a}_j \tag{8}$$

in which the first term denotes the classical finite element approximation which is composed by the derivatives of shape functions in whole domain and the second term presents the derivative of enriched shape functions which is constructed in the domain of set $\mathbf{n}_\psi$. Thus, the well known strain matrix relating the increments of strain and displacement can be written as

$$\mathbf{B}_i^u = \begin{bmatrix} \frac{\partial N_i}{\partial x} & 0 \\ 0 & \frac{\partial N_i}{\partial y} \\ \frac{\partial N_i}{\partial y} & \frac{\partial N_i}{\partial x} \end{bmatrix}, \qquad \mathbf{B}_i^a = \begin{bmatrix} \frac{\partial}{\partial x}\left(N_i \left| \sum_k N_k \psi_k \right| \right) & 0 \\ 0 & \frac{\partial}{\partial y}\left(N_i \left| \sum_k N_k \psi_k \right| \right) \\ \frac{\partial}{\partial y}\left(N_i \left| \sum_k N_k \psi_k \right| \right) & \frac{\partial}{\partial x}\left(N_i \left| \sum_k N_k \psi_k \right| \right) \end{bmatrix} \tag{9}$$

On substituting the trial function of Eq. (7) into the weak form of equilibrium equation of elasto-plasticity, i.e.,

$$\int_\Omega \boldsymbol{\sigma} : \boldsymbol{\varepsilon}(\mathbf{u}) \, \mathrm{d}\Omega = \int_\Omega \mathbf{b}\mathbf{u} \, \mathrm{d}\Omega + \int_\Gamma \mathbf{t}\mathbf{u} \, \mathrm{d}\Gamma \tag{10}$$

the discrete system of equations can be obtained as $\mathbf{K}\mathbf{d} = \mathbf{f}$, where $\mathbf{d}$ is the vector of unknowns of $\mathbf{u}_i$ and $\mathbf{a}_j$ at the nodal points, and $\mathbf{K}$ and $\mathbf{f}$ are the global stiffness matrix and external force vector, defined as

$$\mathbf{K}_{ij} = \begin{bmatrix} \mathbf{K}_{ij}^{uu} & \mathbf{K}_{ij}^{ua} \\ \mathbf{K}_{ij}^{au} & \mathbf{K}_{ij}^{aa} \end{bmatrix}, \qquad \mathbf{f}_i = \{ \mathbf{f}_i^u \mathbf{f}_i^a \}^{\mathrm{T}} \tag{11}$$

where

$$\begin{aligned} \mathbf{K}_{ij}^{\alpha\beta} &= \int_{\Omega^e} (\mathbf{B}_i^\alpha)^{\mathrm{T}} \mathbf{D}^{\mathrm{ep}} (\mathbf{B}_j^\beta) \, \mathrm{d}\Omega \quad (\alpha, \beta = u, a) \\ \mathbf{f}_i^\alpha &= \int_{\Omega^e} N_i^\alpha \mathbf{b} \, \mathrm{d}\Omega + \int_{\Gamma^e} N_i^\alpha \mathbf{t} \, \mathrm{d}\Gamma \quad (\alpha = u, a) \end{aligned} \tag{12}$$

where $\mathbf{D}^{\mathrm{ep}}$ is the elasto-plastic constitutive matrix. In Eq. (12), $N_i^\alpha \equiv N_i$ is for a finite element displacement degree of freedom, and $N_i^\alpha \equiv N_i \psi$ for an enriched degree of freedom.

It must be noted that for the elements cut by the interface boundary, the standard Gauss quadrature points are insufficient for numerical integration, and may not adequately integrate the discontinuous field. If the integration of the discontinuous enrichment is indistinguishable from that of a constant function, the system of equations may be rank deficient. Thus, it is necessary to modify the element quadrature points to accurately evaluate the contribution to the weak form for both sides of discontinuity. In what follows, we present the modifications made to the numerical integration scheme for elements cut by a discontinuity surface.

The discrete weak form is normally constructed with a loop over all elements, as the domain is approximated by

$$\Omega = \bigcup_{e=1}^{m} \Omega_e \tag{13}$$

where m is the number of elements and Ω_e is the element sub-domain. For the elements located on interface boundary, an appropriate procedure is performed by dividing the elements into triangular sub-domains Ω_s with boundaries aligned with the discontinuity surface geometry, i.e.,

$$\Omega_e = \bigcup_{s=1}^{m_s} \Omega_s \tag{14}$$

where m_s denotes the number of sub-polygons of the element. The Gauss points of sub-triangles are used for numerical integration across the contact surface, as shown in Fig. 2. Different algorithms may be applied to generate these sub-polygons, based on sub-triangles and sub-quadratics. In this study, sub-triangles are implemented for numerical integration. It is essential to mention that these sub-polygons only generated for numerical integration and no new degrees of freedom are added to system. In the construction of the matrix equations, the element loop is replaced by a loop over the sub-triangles for those elements cut by the discontinuity.

4. Modeling frictional contact with the X-FEM

Numerical simulation of frictional contact in FEM can be achieved by employing contact elements. Although these elements have wide application in simulation of contact problems, the modeling of evolving contact surfaces with the finite element method is cumbersome due to the need to update the mesh topology to match the geometry of the contact surface, and implement the contact elements between two different bodies. The extended finite element method alleviates much of the burden associated with mesh generation by not requiring the finite element mesh to conform to contact surfaces, and in addition, provides a seamless means to use higher-order elements or special finite elements without significant changes in the formulation. Here, the plasticity formulation of X-FEM has been simultaneously applied with an iterative procedure, called LATIN method (Ladeveze, 1998), to insert the nonlinear boundary conditions along the contact surface. Similar algorithm was applied by Dolbow et al. (2001) in modeling crack growth, in which the nonlinear behavior of frictional contact was separated from the linear governing equations.

Consider that Γ_c be a contact surface between the tool and powder in domain Ω, as shown in Fig. 1(a). The interface Γ_c is distinguished into two parts Γ_c^+ and Γ_c^- in which $\Gamma_c = \Gamma_c^+ \cup \Gamma_c^-$ and the normal vector to Γ_c^+ denoted by $\mathbf{n}$. We also introduce the displacement and traction on each face of the contact surface by $\boldsymbol{w}^+$, $\mathbf{t}^+$ on Γ_c^+ and $\boldsymbol{w}^-$, $\mathbf{t}^-$ on Γ_c^-. In order to obtain an appropriate form that is suitable for numerical treatment of contact behavior, the weak form of equilibrium Eq. (10) can be rewritten as

$$\int_\Omega \boldsymbol{\sigma} : \boldsymbol{\varepsilon}(\mathbf{u})\,\mathrm{d}\Omega = \int_\Omega \mathbf{b}\mathbf{u}\,\mathrm{d}\Omega + \int_{\Gamma_t} \mathbf{t}\mathbf{u}\,\mathrm{d}\Gamma + \int_{\Gamma_c} \mathbf{t}\boldsymbol{w}\,\mathrm{d}\Gamma \tag{15}$$

in which the last term represents the concept of energy, dissipated in the relative motion of two sides of the contact surface along each other, where

$$\int_{\Gamma_c} \mathbf{t}\cdot\boldsymbol{w}\,\mathrm{d}\Gamma = \int_{\Gamma_c^+} \mathbf{t}^+\cdot\boldsymbol{w}^+\,\mathrm{d}\Gamma + \int_{\Gamma_c^-} \mathbf{t}^-\cdot\boldsymbol{w}^-\,\mathrm{d}\Gamma \tag{16}$$

It is important that the displacement field of domain $\mathbf{u}$ and the displacement on contact surface $\boldsymbol{w}$ be kinematically admissible, i.e., $\mathbf{u}|_{\Gamma_c^+} = \boldsymbol{w}^+$ and $\mathbf{u}|_{\Gamma_c^-} = \boldsymbol{w}^-$. The interfacial constitutive law on the contact surface can be expressed in terms of the displacement and traction $(\boldsymbol{w},\mathbf{t})$ on both sides of the contact surface by $\mathscr{F}(\boldsymbol{w}^+,\boldsymbol{w}^-,\mathbf{t}^+,\mathbf{t}^-)=0$, with $\mathscr{F}$ denoting the friction constitutive law that indicates the stress level at which relative slip motion occurs. The goal is to obtain the stress and displacement fields on both sides of contact surface which satisfy the equilibrium and consistency conditions. In this study, the LATIN method is applied by decomposing the governing equations into a set $\boldsymbol{A}$ which is related to the global system, and a set $\boldsymbol{I}$ of local system which is related to contact problem. The sets $\boldsymbol{A}$ and $\boldsymbol{I}$ can be defined as follows:

$$\boldsymbol{A} = \{\boldsymbol{s}\in\Re^2 : \boldsymbol{\sigma} = \mathbf{D}^{\mathrm{ep}}\boldsymbol{\varepsilon}(\mathbf{u}) \text{ and } F(\boldsymbol{\sigma},\kappa)=0 \text{ on } \Omega\} \tag{17}$$

$$\boldsymbol{I} = \{\boldsymbol{s}\in\Re^2 : \mathscr{F}(\boldsymbol{w}^+,\boldsymbol{w}^-,\mathbf{t}^+,\mathbf{t}^-)=0 \text{ on } \Gamma_c\} \tag{18}$$

where $\boldsymbol{s}=(\mathbf{u},\boldsymbol{\sigma},\boldsymbol{w},\mathbf{t})$.

In order to obtain the value of $\boldsymbol{s}^{AI}$, which is located at the intersection of the sets $\boldsymbol{A}$ and $\boldsymbol{I}$, the iterative strategy of LATIN method is applied at each increment of governing equations of global system within the time

step (t_n, t_{n+1}) in the following manner. The iteration begins with an initial value of $\boldsymbol{s}_0^A$ in $\boldsymbol{A}$. The value of $\boldsymbol{s}_0^I$ can be then obtained by satisfying the governing equation of set $\boldsymbol{I}$. In the next step, the governing equations of set $\boldsymbol{A}$ is preserved for obtaining the value of $\boldsymbol{s}_1^A$. This procedure is carried out until the convergence is obtained. In this algorithm, the value of $\boldsymbol{s}_{i+1}^A$ at iteration $i+1$ can be calculated from $\boldsymbol{s}_i^A$ at iteration i in two steps; first $\boldsymbol{s}_i^A$ to $\boldsymbol{s}_i^I$ and then, $\boldsymbol{s}_i^I$ to $\boldsymbol{s}_{i+1}^A$ by satisfying the governing equations of set $\boldsymbol{I}$ and $\boldsymbol{A}$, respectively. The iteration will be stopped when the difference between $\boldsymbol{s}_i^I$ and $\boldsymbol{s}_{i+1}^A$ is below a specified tolerance. It must be noted that going from one set of equation to the other set requires having extra equations in order to achieve the fast convergence (Dolbow et al., 2001).

Finally, in order to compute the total stiffness matrix, the integral term of contact behavior in the weak form of Eq. (15) is incorporated into the discretized equations of global system. The stiffness matrix of global system is therefore combined with the stiffness matrix due to contact problem, yielding a system of algebraic equations defined as $(\mathbf{K}_A + \mathbf{K}_I)\mathbf{d} = \mathbf{f}$, with $\mathbf{K}_A$ denoting the stiffness matrix of global system and $\mathbf{K}_I$ the stiffness matrix due to contact behavior. The procedure for constructing the stiffness matrix $\mathbf{K}_A$ is similar to that explained in Section 3—however, the enrichment function of level set method is replaced by the Heaviside function in order to approximate the displacement field of the elements located on contact surface. The procedure for construction of the stiffness matrix $\mathbf{K}_I$ is carried out based on the one-dimensional integration of related functions on the contact surface Γ_c. In this case, the interface is partitioned into a set of one-dimensional segments, which are similar to the two-dimensional sub-triangles used for the volume integral. The numerical integration of $\mathbf{K}_I$ is then performed using the Gauss quadrature points along each of one-dimensional segments.

4.1. Friction constitutive model

The objective of the constitutive model of friction is to provide a theoretical description of motion at the interface of bodies in contact. The plasticity theory of friction can be achieved by an analogy between plastic and frictional phenomena. In order to formulate such a theory of friction several requirements have to be considered (Khoei and Nikbakht, 2005). These requirements, which are similar to the requirements considered in the theory of elasto-plasticity, are as follows: stick (or adhesion) law, stick–slip law, wear and tear rule, slip criterion, and slip rule.

Consider $\boldsymbol{w}^-$ and $\boldsymbol{w}^+$ be the displacements on each face of the contact surface on Γ_c, the relative displacement between two surfaces can be defined by $g_N(\boldsymbol{x}) = (\boldsymbol{w}^- - \boldsymbol{w}^+)\mathbf{n}$, with $g_N(\boldsymbol{x})$ denoting the gap between the two bodies and $\mathbf{n}$ the normal vector to the interface Γ_c^+. During the contact and sliding of the bodies, we define p_N and p_T as the normal and tangential load acting on the point $\boldsymbol{x}$, respectively. The contact conditions is expressed in the standard Kuhn–Tucker form as

$$g_N \geqslant 0, \qquad p_N \leqslant 0, \qquad p_N g_N = 0 \tag{19}$$

where $p_N = \mathbf{t}^+\mathbf{n}$ and $p_T = \mathbf{n} \otimes (\mathbf{t}^+ \otimes \mathbf{n})$, in which the normal and tangential components must be in equilibrium on both sides of contact surface. Consider that there is no gap between the two bodies in the sliding contact problem, and the tangential displacement consists of stick and slip decompositions, which is in principle the same as the decomposition of elastic and plastic behavior. Thus, the decomposition of the tangential displacement at the contact surface can be expressed by $\boldsymbol{w}_T = \boldsymbol{w}_T^{\mathrm{e}} + \boldsymbol{w}_T^{\mathrm{p}}$, with $\boldsymbol{w}_T$ denoting the tangential part of the displacement, i.e., $\boldsymbol{w}_T = (\mathbf{I} - \mathbf{n} \otimes \mathbf{n})\boldsymbol{w}$.

In relation (19), the kinetic constraint of impenetrability of two bodies can be satisfied as well as the static condition of compressive normal load. In order to resolve the resulting unilateral contact problem the penalty method is used here, in which the method needs no additional variable as the impenetrability condition is approximately satisfied. Therefore, the normal load $\mathbf{p}_N$ can be obtained from multiplication of the penalty factor k_N and the displacement in the normal direction $\boldsymbol{w}_N$. Similarly, the stick (or elastic) component of the tangential load can be obtained by multiplying the penalty factor k_T and elastic part of the displacement in the tangential direction $\boldsymbol{w}_T^A$. The penalty factors k_N and k_T can be considered as being the normal stiffness constant and shear stiffness constant, respectively. Constitutive laws for the contact loads can now be summarized by $\mathbf{p}_N = \mathbf{k}_N \boldsymbol{w}^{\mathrm{e}}$ and $\mathbf{p}_T = \mathbf{k}_T \boldsymbol{w}^{\mathrm{e}}$, with $\mathbf{k}_N$ and $\mathbf{k}_T$ denoting the normal and tangential parts of the elastic modulus tensor defined as

$$\mathbf{k}_N = -k_N(\mathbf{n}\otimes\mathbf{n}) \tag{20}$$

$$\mathbf{k}_T = -k_T(\mathbf{I}-\mathbf{n}\otimes\mathbf{n}) \tag{21}$$

In order to perform the additive decomposition of displacement into adherence and slip, a slip criterion must be introduced. To this end the slip surface $\mathscr{F}$ is postulated in the contact stress space on which slip will occur. The slip criterion is expressed based on the Coulomb law as

$$\mathscr{F} = \|\mathbf{p}_T\| - \mu_f\|\mathbf{p}_N\| \begin{cases} = 0 & \text{slip (or grap)} \\ < 0 & \text{adherence} \end{cases} \tag{22}$$

where μ_f is the friction coefficient of contact surface. It must be noted that the associated flow rule of slip criterion (22) would generate a normal force. In order to avoid the slave body separation from the contacting surface, a non-associated flow rule is typically adopted (Curnier, 1984). Hence, the slip potential Z is introduced as a cylinder with radius $\|\mathbf{P}_T\|$ for isotropic frictional contact and the slip direction is defined as the outward normal to the slip potential Z. Consequently, the plastic part of the tangential displacement $\boldsymbol{w}_T^{\mathrm{p}}$ can be defined by the definition of the slip rule as

$$\boldsymbol{w}_T^{\mathrm{p}} = \lambda\frac{\partial Z}{\partial \mathbf{p}_T} = \lambda\frac{\mathbf{p}_T}{\|\mathbf{p}_T\|} \tag{23}$$

where λ is a constant multiplier. The constitutive model for the contact problem with a nonlinear frictional evolution law is conveniently described by Eqs. (19)–(23) implemented into the X-FEM formulation.

5. Cap plasticity model

A generalized cap model, based on classical plasticity theory, originally proposed by DiMaggio and Sandler (1971) and Sandler and Baron (1979), allows the control of dilatancy by means of a hardening cap that intersects a fixed failure envelope in a non-smooth fashion. A commonly accepted interpretation of this model, given by Simo et al. (1988) and Hofstetter et al. (1993), assumes a one-to-one correspondence between the hardening of the cap and the plastic volume change. However, if a one-to-one hardening law is postulated, softening response may occur when the stress point is located at the compressive corner region. Motivated by this softening behavior, Sandler and Rubin (1979) proposed a modified hardening law which prevents softening response. The generalized cap models have also been expanded by Nelson and Baladi (1977) to include rate effects, and anisotropic behavior within the yield surface and visco-plastic behavior during yielding.

The cap models are based on the concept of continuous yielding of materials, but they are expressed in terms of a three-dimensional state of stress and are formulated on the basis of consistent mechanics principles (Khoei et al., 2004). The yield surface of this elasto-plastic model has a moving cap, intersecting the hydrostatic loading line, whose position is a function of plastic volumetric strain (Fig. 4). The main features of the cap model include a failure surface and an elliptical yield cap which closes the open space between the failure surface and the hydrostatic axis. The cap surface expands in the stress space according to a specified hardening rule. The functional forms for these surfaces are

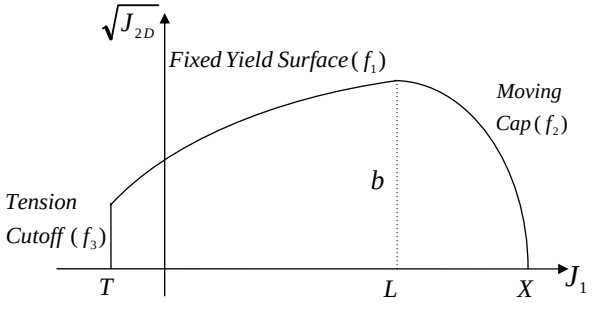

Fig. 4. The double-surface cap plasticity model.

$$f_1 = \sqrt{J_{2D}} - \theta J_1 + \gamma e^{-\beta J_1} - \alpha = 0 \tag{24}$$

$$f_2 = R^2 J_{2D} + (J_1 - L)^2 - R^2 b^2 = 0 \tag{25}$$

$$f_3 = J_1 - T = 0 \tag{26}$$

where J_1 and J_{2D} are the first invariant of effective stress tensor and second invariant of deviatoric effective stress tensor, respectively. α, β, γ and θ are the parameters of fixed yield surface f_1, which controls the deviatoric stress limits. The fixed yield surface f_1 is defined by an exponential function and in reality is consist of two different Drucker–Prager yield surfaces. The cap yield surface f_2 is an elliptical function, with R denoting the ratio of two elliptical cap's diameters. The function f_3 indicates the tension cut-off zone, with T denoting the material's tension limit.

The hardening rule for moving cap is related to the volumetric plastic strain ε_v^p as

$$X(\kappa) = X(\varepsilon_v^p) = \frac{-1}{D} \ln\left(1 - \frac{\varepsilon_v^p}{W}\right) + X_0 \tag{27}$$

where D and W are material parameters and X_0 refers to the position of initial cap surface. The plastic hardening/softening modulus H is zero for f_1 and f_3. Fig. 5 shows how the cap yield surface grows with densification due to increase of the volumetric plastic strain. The 3D representation of the double-surface plasticity is shown in Fig. 6 for different values of volumetric plastic strain.

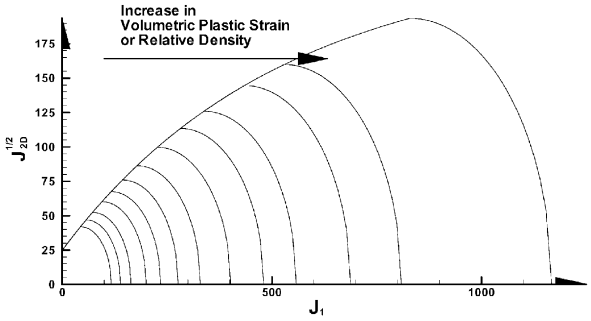

Fig. 5. The expansion of moving cap surface with increasing the volumetric plastic strain, or relative density.

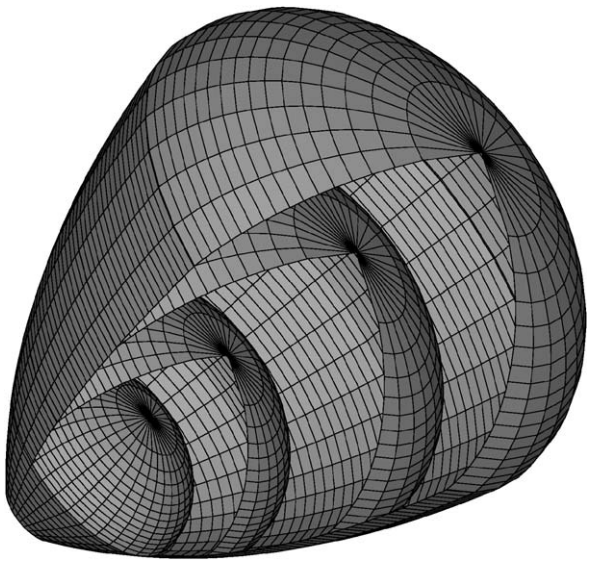

Fig. 6. 3D representation of cap plasticity model.

5.1. Computational algorithm of cap model

The cap plasticity model presented here is based on the concept of generalized plasticity theory in which the elasto-plastic constitutive matrix is defined by

$$\mathbf{D}^{\mathrm{ep}} = \mathbf{D}^{\mathrm{e}} - \frac{\mathbf{D}^{\mathrm{e}}\mathbf{n}_Q\mathbf{n}_F^{\mathrm{T}}\mathbf{D}^{\mathrm{e}}}{H + \mathbf{n}_F^{\mathrm{T}}\mathbf{D}^{\mathrm{e}}\mathbf{n}_Q} \tag{28}$$

where $\mathbf{D}^{\mathrm{e}}$ is the elastic constitutive matrix ($\mathrm{d}\boldsymbol{\sigma}^{\mathrm{e}} = \mathbf{D}^{\mathrm{e}}\mathrm{d}\boldsymbol{\varepsilon}$), H is the plastic hardening/softening modulus, $\mathbf{n}_F$ is the normal vector to yield surface ($\partial F/\partial\boldsymbol{\sigma}$) and $\mathbf{n}_Q$ is the normal vector to plastic potential surface ($\partial Q/\partial\boldsymbol{\sigma}$). In order to compute the elasto-plastic constitutive matrix, we need to calculate the plastic hardening/softening modulus and flow direction vector (Khoei, 2005).

$$H = -\left(\frac{\partial f_2}{\partial\kappa}\right)\left(\frac{\partial\kappa}{\partial\boldsymbol{\varepsilon}}\right)^{\mathrm{T}}\mathbf{n}_Q \tag{29}$$

$$\frac{\partial F}{\partial\boldsymbol{\sigma}} = C_1\frac{\partial J_1}{\partial\boldsymbol{\sigma}} + C_2\frac{\partial(J_{2\mathrm{D}})^{1/2}}{\partial\boldsymbol{\sigma}} + C_3\frac{\partial J_{3\mathrm{D}}}{\partial\boldsymbol{\sigma}} \tag{30}$$

where $C_1 = \partial F/\partial J_1$, $C_2 = \partial F/\partial(J_{2\mathrm{D}})^{1/2}$ and $C_3 = \partial F/\partial J_{3\mathrm{D}}$.

For the fixed yield surface, the values of constants C_1, C_2 and C_3 in the case of associated flow rule are as follows:

$$C_1 = -\theta - \beta\gamma\mathrm{e}^{-\beta J_1}, \qquad C_2 = 1, \qquad C_3 = 0 \tag{31}$$

In above relations, the value of C_1 is less than zero. It means that the normal vector to the plastic potential surface is in opposite direction of J_1-axis. On the other hand, the associated flow rule results in dilation of material (increase of volume) and the stress state lays on the fixed yield surface at the ultimate shear stress. As the ultimate shear stress shows no volume changes in material, the non-associated flow rule can be therefore utilized, in which the normal vector to the plastic potential surface is perpendicular to J_1-axis. Thus, the values of constants C_1, C_2 and C_3 for plastic flow vector $\mathbf{n}_Q$ are

$$C_1 = 0, \qquad C_2 = 1, \qquad C_3 = 0 \tag{32}$$

In order to calculate the values of constants C_1, C_2 and C_3 and parameter of hardening/softening modulus H for moving cap surface, function f_2 in Eq. (25) is rewritten as

$$\sqrt{R^2J_{2\mathrm{D}} + (J_1 - L)^2} - Rb = 0 \tag{33}$$

Thus, the values of constants C_i in flow direction vector are

$$C_1 = \frac{J_1 - L}{\sqrt{R^2J_{2\mathrm{D}} + (J_1 - L)^2}}, \qquad C_2 = \frac{R^2\sqrt{J_{2\mathrm{D}}}}{\sqrt{R^2J_{2\mathrm{D}} + (J_1 - L)^2}}, \qquad C_3 = 0 \tag{34}$$

The plastic hardening/softening modulus can be determined by Eq. (29). Considering the hardening parameter κ equal to $\varepsilon_v^{\mathrm{p}}$, it leads to

$$H = -\left(\frac{\partial f_2}{\partial\varepsilon_v^{\mathrm{p}}}\right)\left(\frac{\partial\varepsilon_v^{\mathrm{p}}}{\partial\boldsymbol{\varepsilon}}\right)^{\mathrm{T}}\mathbf{n}_Q = -\left(\frac{\partial f_2}{\partial\varepsilon_v^{\mathrm{p}}}\right)(n_{Qii}) \tag{35}$$

where

$$\frac{\partial f_2}{\partial\varepsilon_v^{\mathrm{p}}} = \frac{\partial f_2}{\partial L}\frac{\partial L}{\partial\varepsilon_v^{\mathrm{p}}} + \frac{\partial f_2}{\partial b}\frac{\partial b}{\partial\varepsilon_v^{\mathrm{p}}} \tag{36}$$

where

$$\frac{\partial f_2}{\partial L} = 2(J_1 - L) \tag{37}$$

$$\frac{\partial f_2}{\partial b} = -2R^2 b \tag{38}$$

From the definition of moving cap surface, we have $L = X - Rb$, $b = \theta L - \gamma e^{-\beta L} + \alpha$ and then, $L(1 + R\theta) - R\gamma e^{-\beta L} + R\alpha = X$. By taking derivative from these relations, we will obtain

$$\frac{\partial L}{\partial \varepsilon_v^p} = \frac{1}{D(W - \varepsilon_v^p)} \frac{1}{1 + R\theta + R\beta\gamma e^{-\beta L}} \tag{39}$$

$$\frac{\partial b}{\partial \varepsilon_v^p} = \frac{1}{R}\left(\frac{\partial X}{\partial \varepsilon_v^p} - \frac{\partial L}{\partial \varepsilon_v^p}\right) \tag{40}$$

Finally, the values of constants C_1, C_2 and C_3 for the tension cut-off yield surface can be simply calculated according to Eq. (26) as

$$C_1 = -1.0, \qquad C_2 = 0, \qquad C_3 = 0 \tag{41}$$

and the plastic hardening/softening modulus for tension cut-off surface is assumed to be zero.

5.2. Parameter determination of cap plasticity

In order to evaluate the parameters of double-surface plasticity, the experimental results of confining pressure and triaxial tests are necessary for parameter determination of the fixed, moving cap and tension cut-off yield surfaces. The fixed yield surface has an exponential form which is composed of an initial portion of the Drucker–Prager envelope joined smoothly to the subsequent Drucker–Prager line, as demonstrated in Fig. 7(a). The slope of the first Drucker–Prager line, i.e., line I, is greater than the slope of the second Drucker–Prager line, i.e., line II. The logic for adopting the second Drucker–Prager surface in higher stresses is based on the observation that at higher stresses the material behave like a liquid. This was adopted particularly to simulate behavior of cohesionless materials subjected to high stresses.

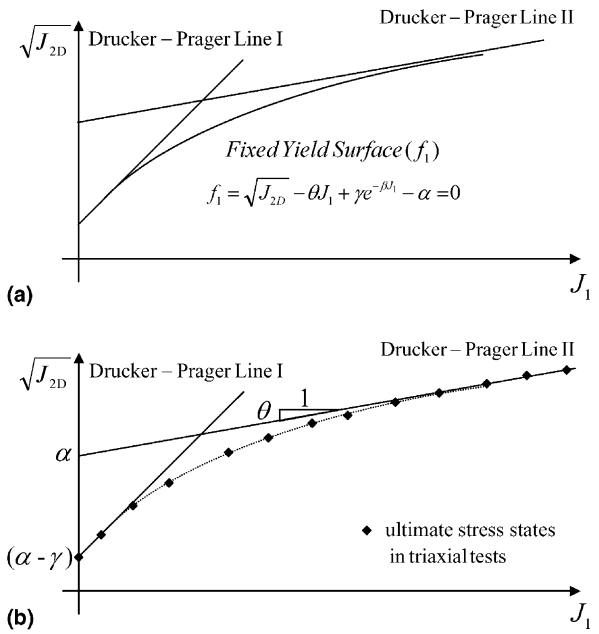

Fig. 7. The fixed yield surface of double-surface plasticity: (a) the model description and (b) the parameter determination.

In order to determine the parameters of fixed yield surface f_1, the results of triaxial tests are necessary at the ultimate shear stresses. These ultimate points are presented in Fig. 7(b) in $J_1 - \sqrt{J_{2D}}$ plane. Considering the state of stress when J_1 is equal to zero and substituting $J_1 = 0$ in Eq. (24) lead to

$$f_1 = \sqrt{J_{2D}} + \gamma - \alpha = 0 \tag{42}$$

It means that the intersection of the fixed yield surface, or the Drucker–Prager line I, with $\sqrt{J_{2D}}$-axis is $\alpha - \gamma$. As β is assumed to be a positive quantity and compression is taken as positive, the quantity of $e^{-\beta J_1}$ will be very small for large value of J_1. Thus, it leads to

$$f_1 = \sqrt{J_{2D}} - \theta J_1 - \alpha = 0 \tag{43}$$

The above equation represents the Drucker–Prager yield criterion, which is shown by line II in Fig. 7. As can be observed the slope of this line is θ and its intersection with $\sqrt{J_{2D}}$-axis is α. The parameter β in fixed yield surface can be evaluated using an arbitrary point on transition curve, as shown in Fig. 7.

In order to determine the parameters of moving cap surface f_2, we need to investigate the plastic deformations under compression. The increase of compression causes the increase of plastic volumetric strain and hence, the expansion of cap surface in J_1-axis. The values of D, W and X_0 are computed by using Eq. (27). The value of X_0 is zero when there is no significant initial yielding cap. For granular and porous materials, there is no significant initial stress and $X_0 = 0$. The values of D and W are obtained from the confining pressure, or hydrostatic pressure test. From these tests, the value of X obtained by Eq. (27) is equal to J_1. The elastic volumetric strain ε_v^e is evaluated from the variation of J_1 with ε_v on unloading portion curve obtained from the hydrostatic pressure test. The plastic volumetric strains ε_v^p can be expressed in terms of total and elastic components of strain as

$$\varepsilon_v^p = \varepsilon_v - \varepsilon_v^e \tag{44}$$

The values of D and W are estimated using the variation of J_1 and X with ε_v^p. The parameter R can be determined using the confining pressure and a set of triaxial tests. For the cap yield surface with a given value of X, the shape of surface can be specified in $J_1 - \sqrt{J_{2D}}$ plane for the same values of plastic volumetric strain from different hydrostatic and triaxial tests.

6. Numerical simulation results

6.1. Tablet pressing process

The first example demonstrates the performance of the X-FEM technique in compaction simulation of tablet pressing process. The geometry is used by Lewis and Khoei (2001) to show the applicability of the large FE formulation in this practical example. The material parameters in the constitutive model are calibrated for a sample of metal powder by fitting the model to reproduce data from isostatic compaction and triaxial tests. The experimental data are gained from a set of compaction experiments on an iron-based powder performed by Doremus et al. (1995). The material parameters for simulation of powder are given in Table 1. The die wall friction is simulated using the Coulomb friction coefficient $\mu = 0.08$. A shaped tablet is compacted by simultaneous action of top and bottom punches. The geometry, boundary conditions and finite element mesh are shown in Fig. 8(a). The component is modeled by an axisymmetric representation, as illustrated in this figure.

Table 1
The material model parameters for the cap plasticity

Fixed yield surface parameters	Cap parameters	Tension cut-off
$\alpha = 225$ MPa	$R = 1.75$	$T = -0.3$ MPa
$\beta = 0.002$ MPa^{-1}	$D = 0.005$ MPa	
$\gamma = 200$ MPa	$W = 0.34$	
$\theta = 0.008$	$X_0 = 1$ MPa	

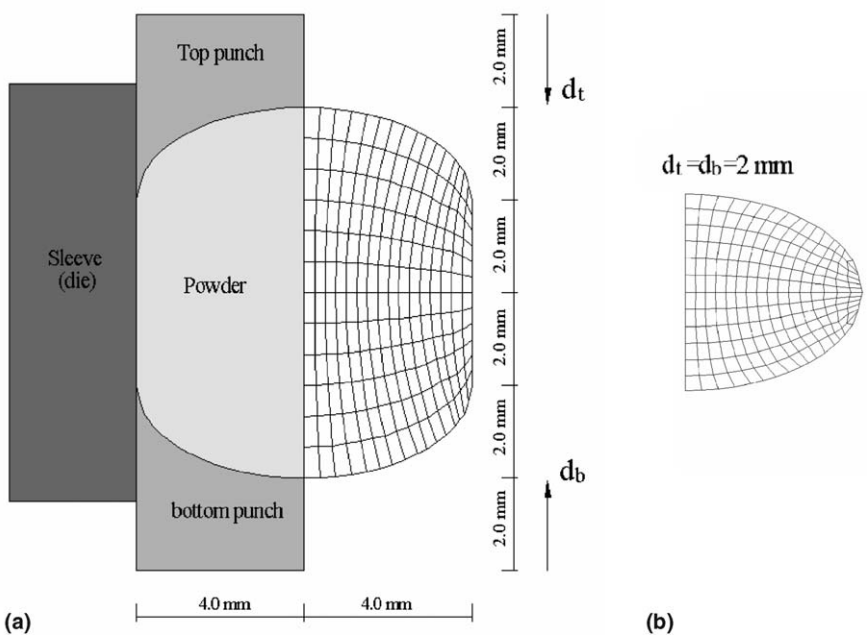

Fig. 8. An axisymmetric shaped tablet component: (a) finite element modeling, geometry and boundary condition and (b) final deformed mesh.

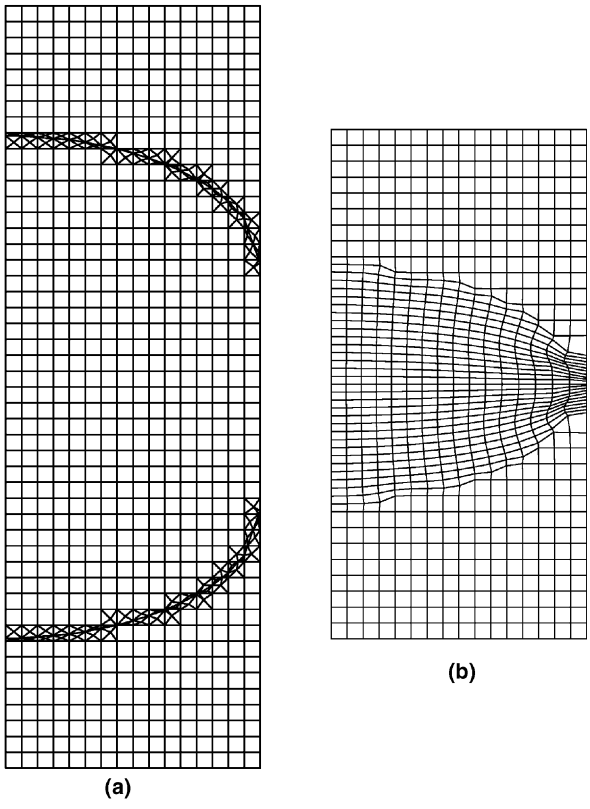

Fig. 9. An axisymmetric shaped tablet component: (a) extended finite element mesh and (b) final deformed mesh.

In FEM mesh, the finite elements are combined with the interface elements along the contact surface. The deformed FE mesh at final stage of compaction is plotted in Fig. 8(b).

In this example, the extended finite element approach is employed to simulate both the highly nonlinear behavior of powder and the contact friction behavior between die and powder. If the discontinuity is as a result of different material properties, then the level set function is proposed as an enrichment function—however, if the discontinuity is due to different displacement fields on either sides of the discontinuity, then the Heaviside function is used. In the X-FEM analysis, the contact friction simulation between die and powder, which are sliding relative to each other is carried out using an iterative procedure of LATIN method. The stick–slip motion is characterized by a periodic switching between sticking and slipping. For those elements which are intersected by the contact surface, the concept of the partition of unity is used to generate the sub-triangles. The Gauss points of sub-triangles are then employed to evaluate the tangent stiffness matrix. In Fig. 9(a), the extended finite element mesh is presented along with the sub-elements used for the partition of unity method. Also plotted in Fig. 9(b) is the deformed mesh at final stage of compaction using X-FEM analysis.

The relative density contours at the four stages of compaction are plotted in Fig. 10 using X-FEM technique. From the contour of final stage of compaction, it can be observed that the density in the right hand region of tablet is greater than other parts while regions with low density appear between high-density regions. In Fig. 11, the normal stress σ_y contours are presented at the four stages of compaction using X-FEM technique. In order to compare the results between two different techniques, the compaction simulation is

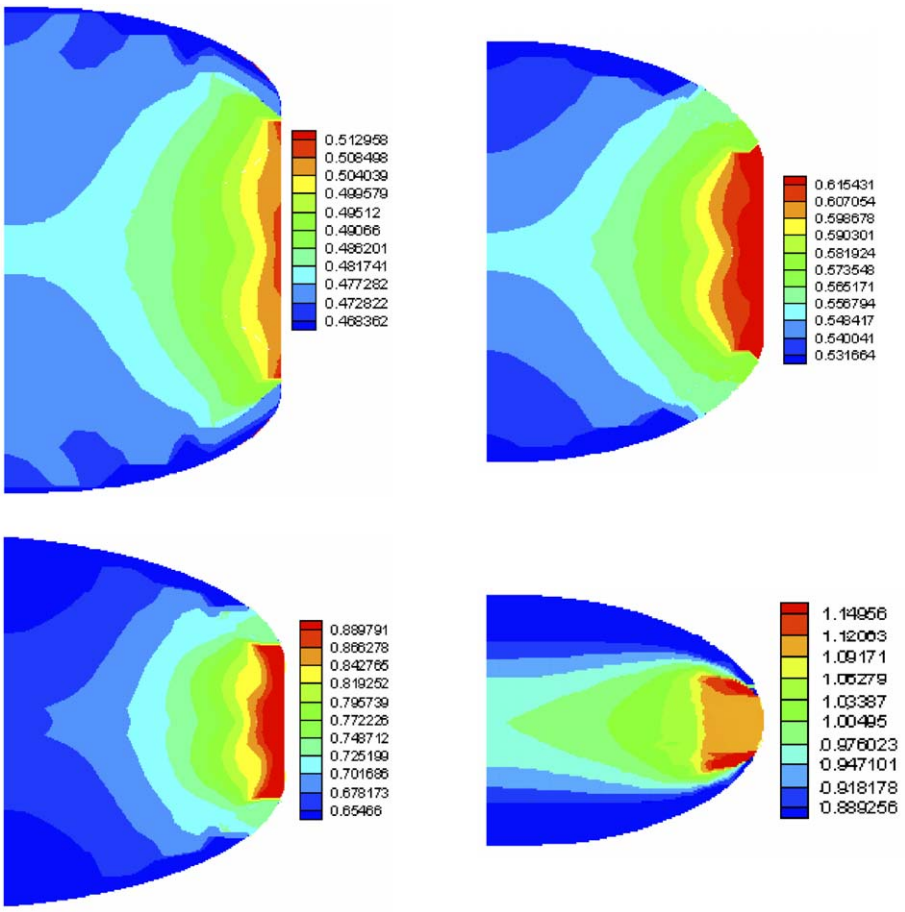

Fig. 10. A shaped tablet component; the density distribution at four stages of compaction using X-FEM technique.

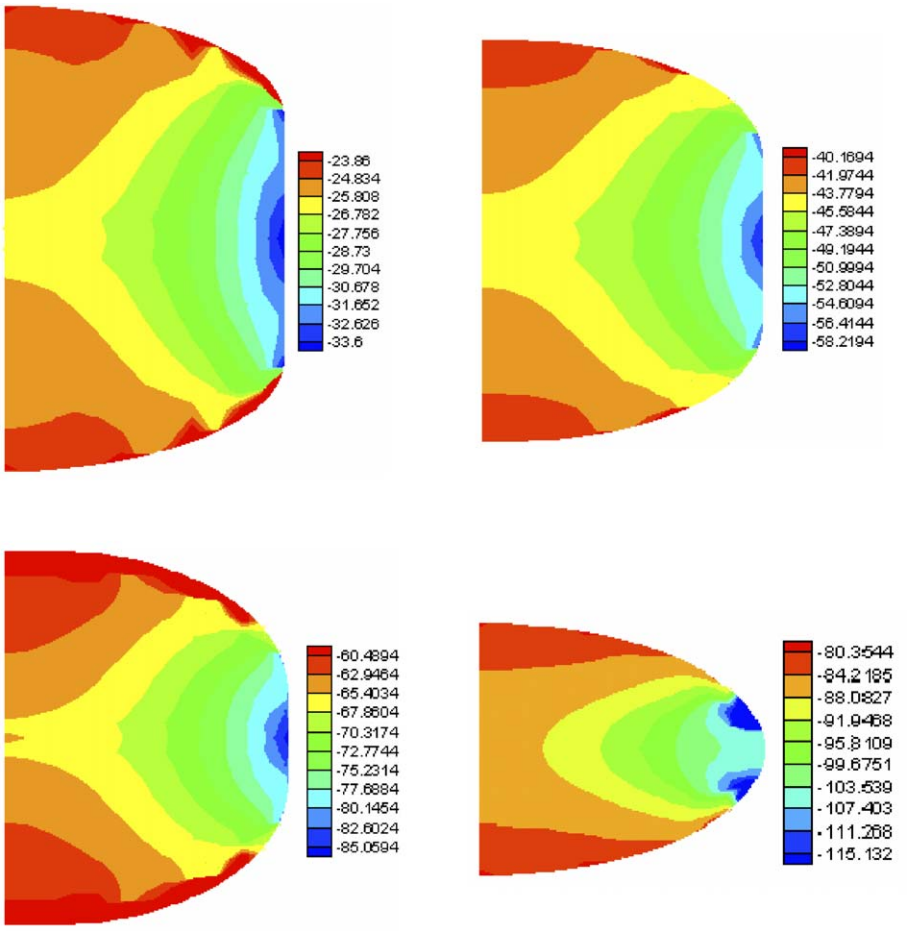

Fig. 11. A shaped tablet component; the normal stress contours at four stages of compaction using X-FEM technique.

performed using a finite element analysis illustrated in Fig. 8. The contours of density distribution and normal stress at the final stage of compaction are shown in Fig. 12. A good agreement can be seen between X-FEM and FEM techniques. The compaction simulation of tablet pressing is also performed by the X-FEM technique considering sleeve, punches and powder, as shown in Fig. 13. This figure presents the final deformed

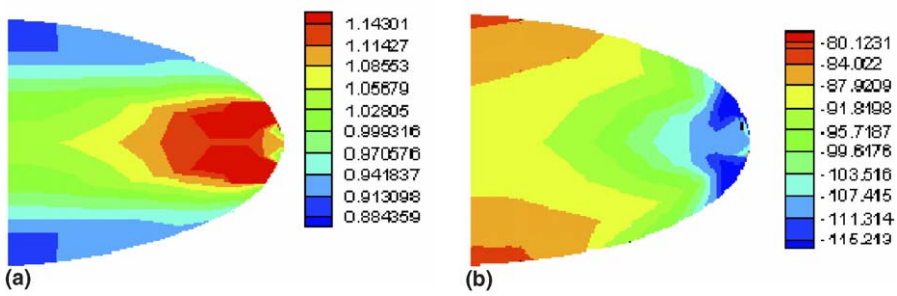

Fig. 12. Modeling of a shaped tablet component using FEM analysis: (a) the final density distribution and (b) the final normal stress contour.

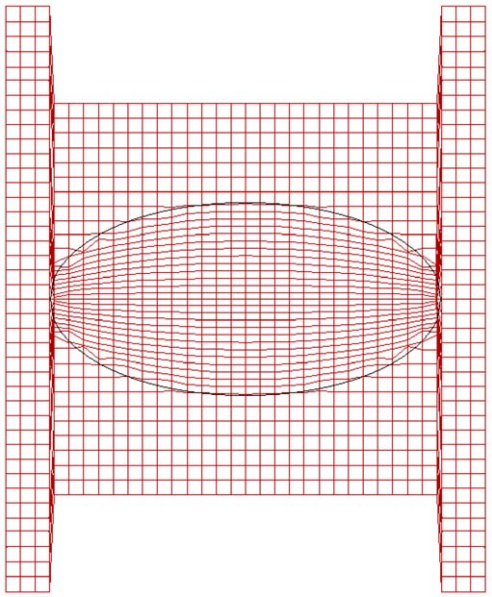

Fig. 13. A shaped tablet component; the final deformed mesh using X-FEM analysis.

mesh for the proposed simulation. It clearly shows how the present X-FEM technique is capable to simulate the plasticity forming of powder compaction with contact friction.

6.2. Compaction of rotational flanged component

The next example refers to the compaction of a flanged component, which is modeled by an axisymmetric representation, as illustrated in Fig. 14(a). Also plotted in this figure are the initial geometry and finite element mesh of component. Numerical simulation is performed using 2D structured mesh of 100 bilinear elements. Material parameters of double-surface plasticity are similar to the first example. The numerical results of finite element simulation were reported by Khoei and Lewis (1999) mesh and Perez-Foguet et al. (2001) and used for comparative purpose. In order to avoid the mesh distortion, as demonstrated by Khoei and Lewis (1999) and Perez-Foguet et al. (2001), simultaneous movements of the top and bottom punches have been applied (the top punch movement of 6.06 mm and the bottom punch movement of 7.7 mm). The friction of powder with punches and die wall are simulated with a Coulomb friction coefficient $\mu = 0.08$.

A rotational flanged component was simulated using a uniform extended finite element mesh of four-noded elements, as shown in Fig. 14(b). In this figure, the mesh is not conformed to the geometry of component and it is substituted by partitioning the domain with some triangular sub-elements. In order to model the discontinuity due to different material properties of powder and punch, the level set method is used as an enrichment function for the elements having discontinuity. To model the discontinuity due to different displacement fields, the Heaviside enrichment function is implemented in simulation of powder-die contact surface. Implementation of these enrichment functions in conjunction with the iterative process of satisfying local and global governing equations in LATIN procedure and recruiting one-dimensional sub-elements in numerical calculations is the procedure of solving this example. Fig. 15 presents the deformed meshes at the half and final stages of compaction using X-FEM technique. The relative density distribution at the half and final movements of punches is presented in Fig. 16. The distribution of relative density is almost homogeneous with difference less than 11% at the final stage of compaction. The higher value of relative density can be seen in bottom corners of component and the lower value in right bottom corner of flange. The relative density distributions are in good agreement with those reported by Perez-Foguet et al. (2001) in Fig. 17. A comparison between the top and bottom punch forces versus vertical displacements obtained by X-FEM and those given by Khoei and Lewis (1999) is illustrated in Fig. 18. It shows a good agreement with finite element analysis.

6.3. Compaction of shaped tip component

The last example refers to the compaction process of a highway-engineering tip, whose axisymmetric geometry is shown in Fig. 1. This example has been experimentally investigated by Haggblad and Oldenburg (1994) and numerically simulated by Khoei and Lewis (1998). The component is composed of discontinuities in geometry which cause some problems in the standard finite element analysis. These difficulties are due to mesh adaption, which is time consuming for the proposed complicated geometry. To overcome these inconveniences, the extended finite element method is employed to remove the mesh conforming to the boundary conditions. In order to illustrate a comparison between the density distribution obtained by the X-FEM model and those obtained using FEM analysis by Khoei and Lewis (1998), the simulation has been performed using the remaining pressing distance from above of 3.0 mm and an under pressing of 1.5 mm. The initial relative density at the start of simulation is 0.25. Material parameters of cap plasticity model chosen for the simulation of powder are given in Table 1. The die wall friction is simulated using the Coulomb friction coefficient $\mu = 0.08$.

In traditional approach, the finite element formulation is characterized by the use of interface elements in which the plasticity theory of friction is incorporated to simulate sliding resistance at the powder–tool

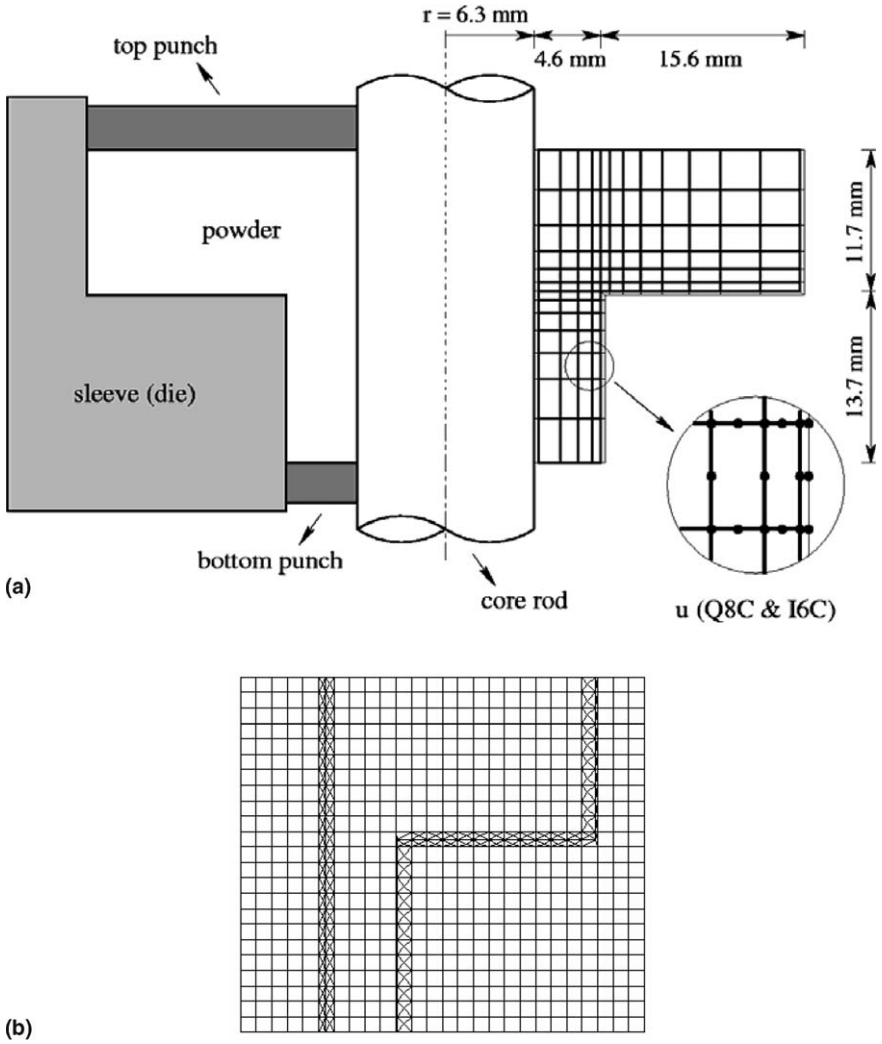

Fig. 14. A rotational flanged component: (a) geometry, boundary condition and finite element mesh and (b) extended finite element mesh.

interface (Khoei and Lewis, 1998). Fig. 19(a) presents the finite element mesh of a shaped tip component using the eight-noded quadrilateral elements. In the present study, we illustrate the performance of X-FEM technique in modeling powder-die friction and highly nonlinear behavior of powder. In Fig. 19(b), a uniform extended finite element mesh of quadratic elements is presented, in which the distinction between punch, sleeve and powder is determined using triangular sub-elements. The deformed FE meshes at the half and final stages of compaction are plotted in Fig. 20. Also plotted in Fig. 21 are the deformed extended FE meshes at the half and final stages of compaction. The relative density distribution at the half and final movements of punches is presented in Fig. 22 using X-FEM technique. The density distributions are in good agreement with those obtained by finite element simulation in Fig. 23. In order to assess the accuracy of the use of X-FEM technique in modeling the complex geometry of tip component, we compare the stress distribution of compacted component using finite element formulation to that obtained by the new technique. Fig. 24(a) presents the normal stress σ_y contour at final stage of compaction using X-FEM technique. This result can be compared with that obtained by FE simulation in Fig. 24(b). Fig. 25 demonstrates a comparison of the variation with time of the

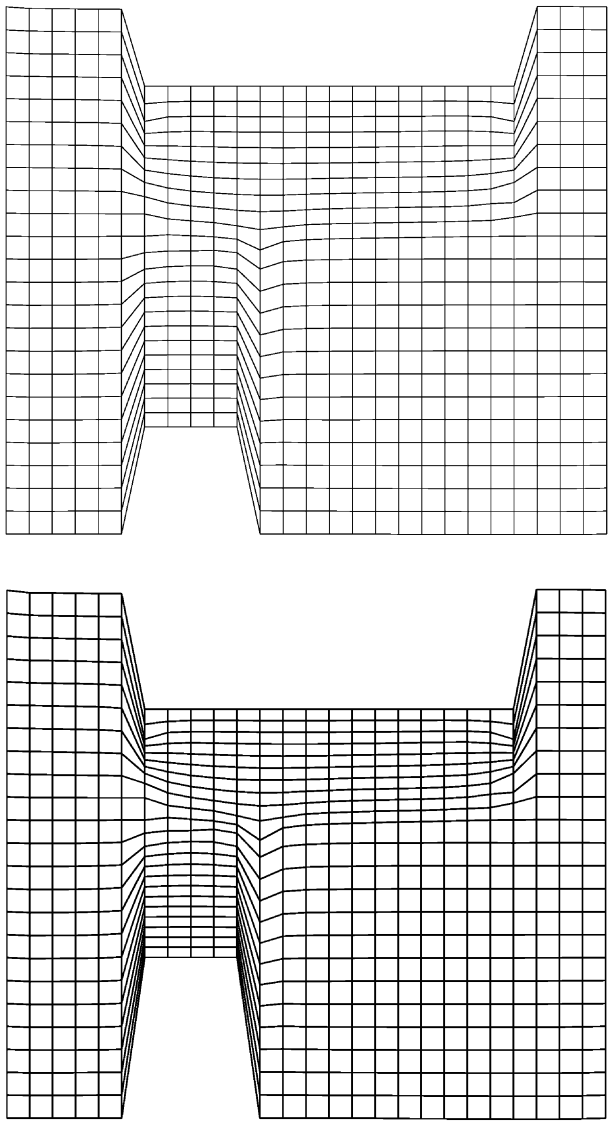

Fig. 15. A rotational flanged component; the deformed meshes at the half and final stages of compaction using X-FEM analysis.

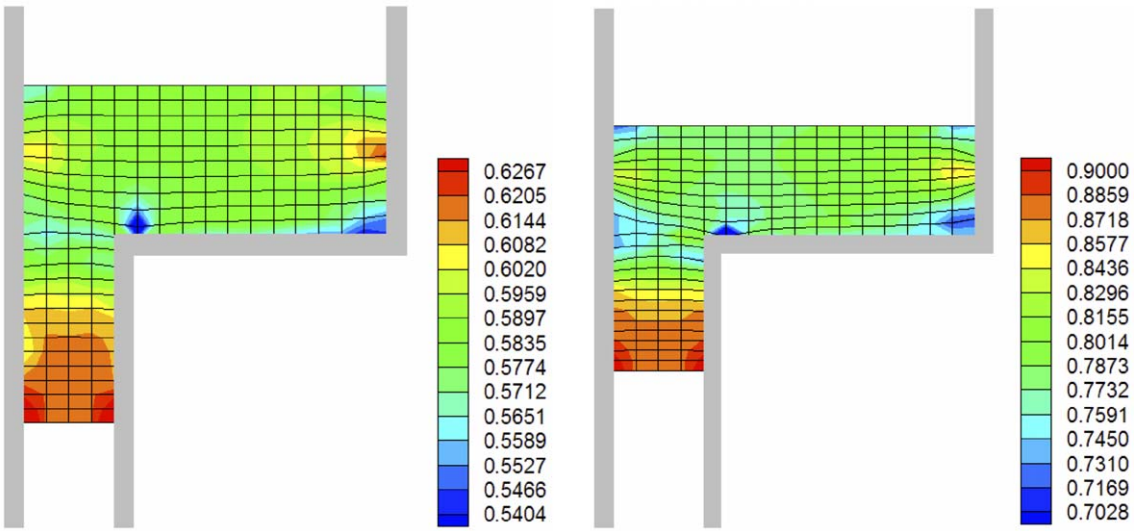

Fig. 16. A rotational flanged component; the density distribution at the half and final stages of compaction using X-FEM analysis.

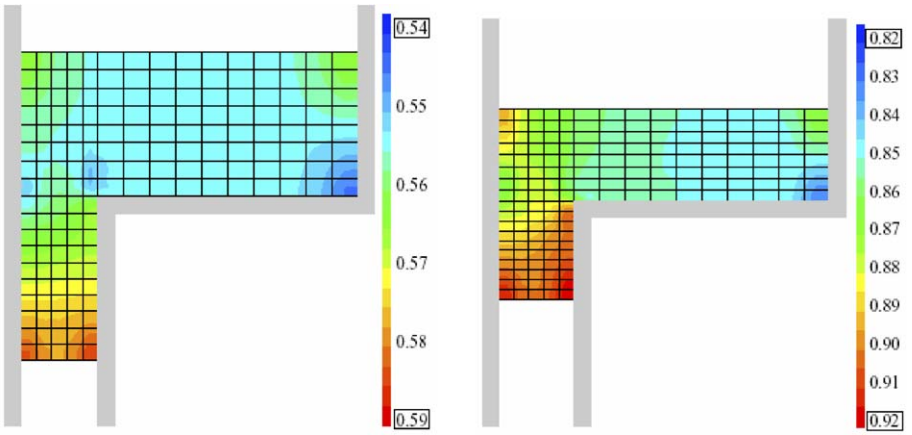

Fig. 17. A rotational flanged component; the density distribution at the half and final stages of compaction using FEM analysis (Perez-Foguet et al., 2001).

relative densities at three different nodes obtained by X-FEM technique and those computed by FEM analysis. A good agreement can be observed between two different techniques.

7. Conclusion

In the present paper, the extended finite element method was presented in pressure-sensitive plasticity of powder compaction considering frictional contact. The technique was applied by employing enrichment functions to approximate the displacement field of the elements located on the interface. The level set function was used for enriching the discontinuities due to different material properties and the Heaviside enrichment function was implemented in simulation of powder-die contact surface. The process was carried out by partitioning the domain with some triangular sub-elements whose Gauss points were used for integration of the domain of the elements. The double-surface cap plasticity model was employed within the X-FEM framework to capture

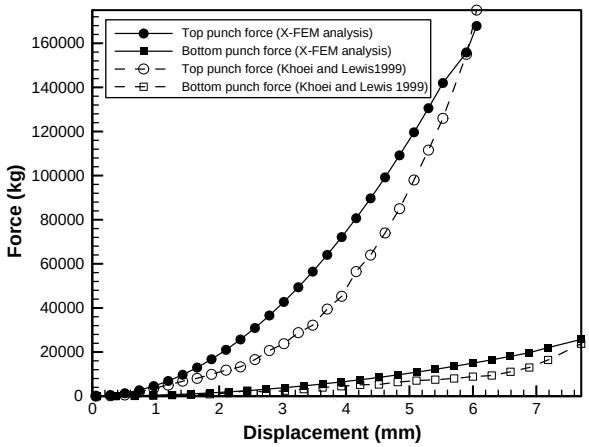

Fig. 18. The top and bottom punch reaction forces at different vertical displacements for a flanged component; a comparison between FEM and X-FEM analysis.

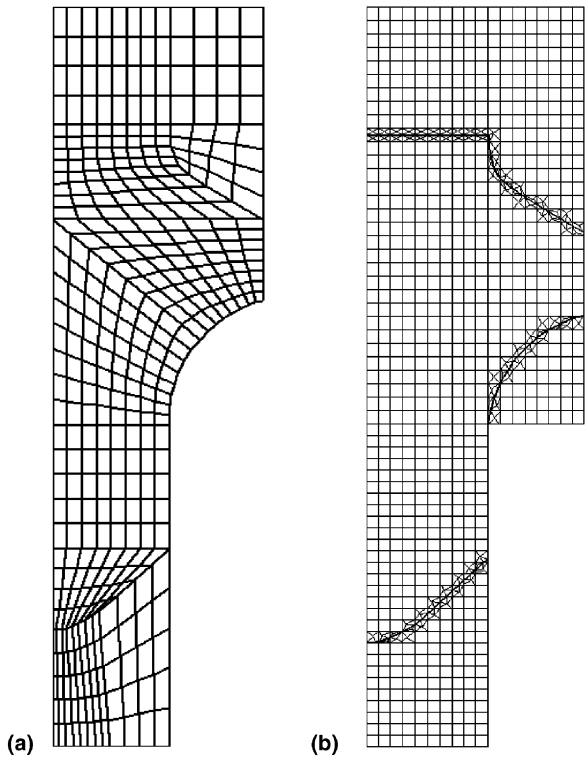

Fig. 19. A shaped tip component: (a) finite element mesh and (b) extended finite element mesh.

the response of initially loose metal powders to complex deformation histories encountered in the compaction process of powder. The plasticity model includes a failure surface and an elliptical cap, which closes the open space between the failure surface and hydrostatic axis. A general algorithm for the cap plasticity from the viewpoint of efficient numerical modeling was presented. The constitutive elasto-plastic matrix and its components were derived, and the procedure for determination of powder parameters was described.

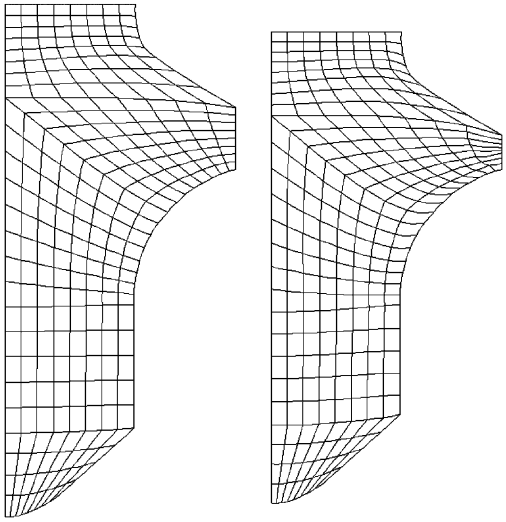

Fig. 20. A shaped tip component; the deformed meshes at the half and final stages of compaction using FEM analysis.

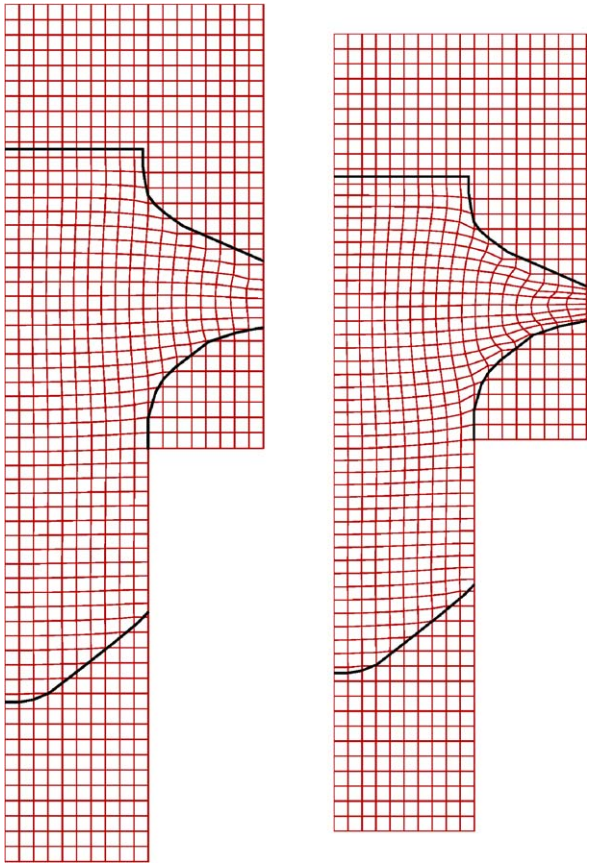

Fig. 21. A shaped tip component; the deformed meshes at the half and final stages of compaction using X-FEM analysis.

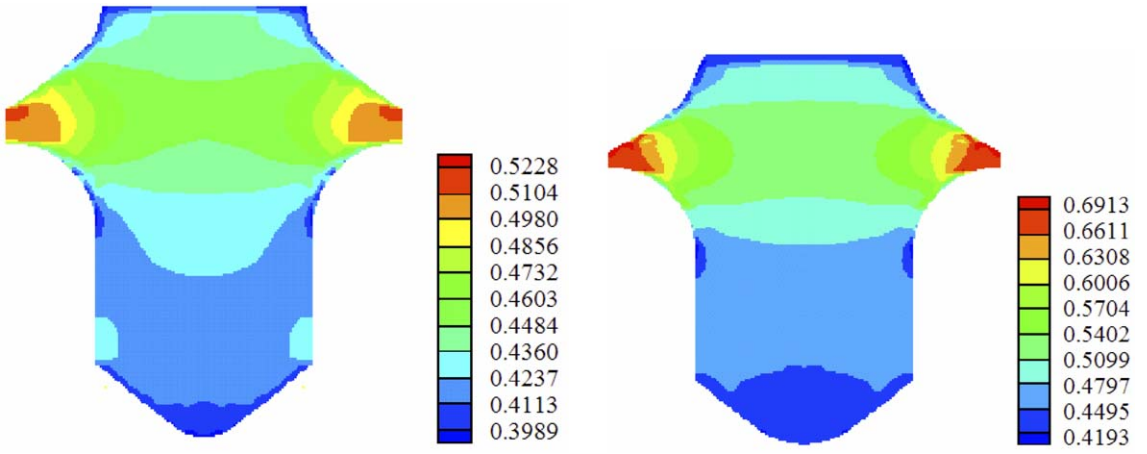

Fig. 22. A shaped tip component; the density distribution at the half and final stages of compaction using X-FEM analysis.

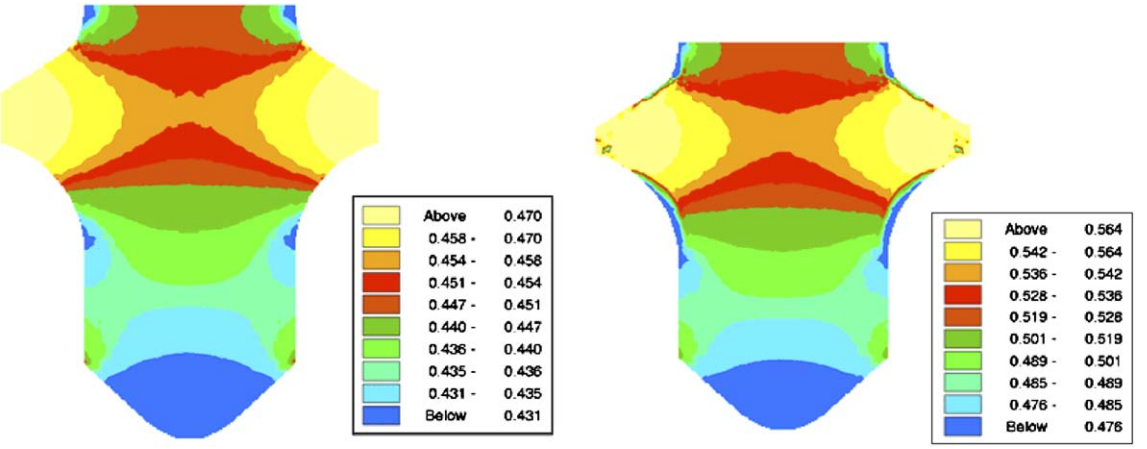

Fig. 23. A shaped tip component; the density distribution at the half and final stages of compaction using FEM analysis.

The plasticity formulation of X-FEM was simultaneously applied with the iterative procedure of LATIN method to insert the nonlinear boundary conditions along the contact surface. The frictional behavior of contact between two bodies was modeled by using the X-FEM technique and applying the Heaviside enrichment function. For the elements located on contact surface, an appropriate procedure was performed by dividing the elements into sub-triangles. The implementation of X-FEM technique was presented in an incremental manner and the role of sub-elements in simulation of contact treatment was demonstrated. Finally, the applicability of the proposed model was demonstrated through several numerical examples with special reference to plasticity forming of powder compaction. The numerical schemes were examined for efficiency in the modeling of a tablet pressing process, the compaction of a rotational flanged component, and compaction forming of a shaped tip component. The simulation of the deformation was shown as well as the distribution of relative densities and stresses using both X-FEM and FEM techniques. A good agreement was achieved between two different techniques. The results clearly indicated that the strategy of adaptive remeshing in powder compaction simulation which consumes high expenses of capacity and time, can be replaced by a new technique based on extended finite element method, which makes it possible to simulate the powder forming problems efficiently and accurately.

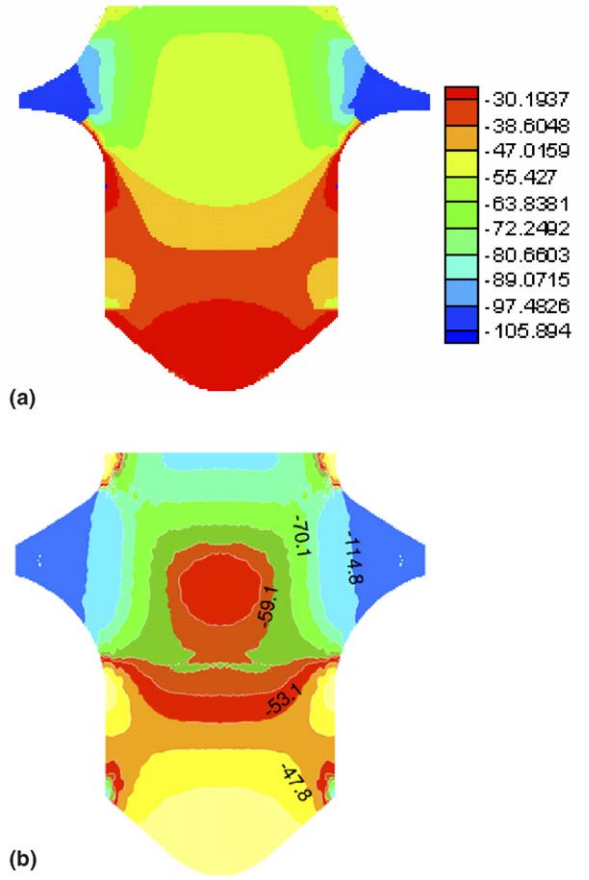

Fig. 24. A shaped tip component; the normal stress contours at the final stage of compaction: (a) X-FEM analysis and (b) FEM analysis.

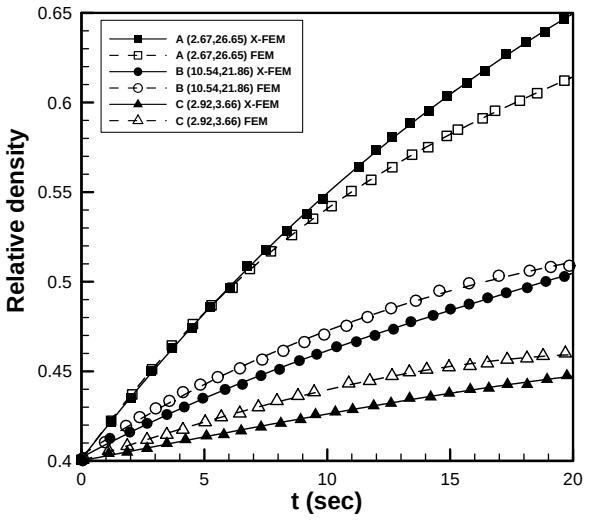

Fig. 25. The variation of relative density with time at different nodes for a shaped tip component; a comparison between FEM and X-FEM analysis.

References

Aydin, I., Briscoe, B.J., Sanliturk, K.Y., 1996. The internal form of compacted ceramic components. A comparison of a finite element modeling with experiment. Powder Tech. 89, 239–254.

Belytschko, T., Black, T., 1999. Elastic crack growth in finite elements with minimal remeshing. Int. J. Numer. Methods Eng. 45, 601–620.

Belytschko, T., Moes, N., Usui, S., Parimi, C., 2001. Arbitrary discontinuities in finite elements. Int. J. Numer. Methods Eng. 50, 993–1013.

Brandt, J., Nilsson, L., 1999. A constitutive model for compaction of granular media, with account for deformation induced anisotropy. Mech. Cohes. Frict. Mater. 4, 391–418.

Brekelmans, W.A.M., Janssen, J.D., Van de Ven, A.A.F., de With, G., 1991. An Eulerian approach for die compaction processes. Int. J. Numer. Methods Eng. 31, 509–524.

Brown, S., Abou-Chedid, G., 1994. Yield behavior of metal powder assemblages. J. Mech. Phys. Solids 42, 383–398.

Brown, S.B., Weber, G.G.A., 1988. A constitutive model for the compaction of metal powders. Modern Dev. Powder Metall. 18, 465–476.

Cedergren, J., Sorensen, N.J., Bergmark, A., 2002. Three-dimensional analysis of compaction of metal powder. Mech. Mater. 34, 43–59.

Chenot, J.L., Bay, F., Fourment, L., 1990. Finite element simulation of metal powder forming. Int. J. Numer. Methods Eng. 30, 1649–1674.

Chessa, J., Belytschko, T., 2003. An enriched finite element method and level sets for axisymmetric two-phase flow with surface tension. Int. J. Numer. Methods Eng. 58, 2041–2064.

Chessa, J., Belytschko, T., 2004. Arbitrary discontinuities in space–time finite elements by level sets and X-FEM. Int. J. Numer. Methods Eng. 61, 2595–2614.

Chessa, J., Smolinski, P., Belytschko, T., 2002. The extended finite element method (XFEM) for solidification problems. Int. J. Numer. Methods Eng. 53, 1959–1977.

Chopp, D.L., Sukumar, N., 2003. Fatigue crack propagation of multiple coplanar cracks with the coupled extended finite element/fast marching method. Int. J. Eng. Sci. 41, 845–869.

Curnier, A., 1984. A theory of friction. Int. J. Solids Struct. 20, 637–647.

Daux, C., Moes, N., Dolbow, J., Sukumar, N., Belytschko, T., 2000. Arbitrary branched and intersecting cracks with the extended finite element method. Int. J. Numer. Methods Eng. 48, 1741–1760.

DiMaggio, F.L., Sandler, I.S., 1971. Material model for granular soils. J. Eng. Mech. Div., ASCE 97, 935–950.

Dolbow, J.E., 1999. An extended finite element method with discontinuous enrichment for applied mechanics, Ph.D. Thesis, Northwestern University.

Dolbow, J., Moes, N., Belytschko, T., 2001. An extended finite element method for modeling crack growth with frictional contact. Comput. Methods Appl. Mech. Eng. 190, 6825–6846.

Doremus, P., Geindreau, C., Martin, A., Debove, L., Lecot, R., Dao, M., 1995. High pressure triaxial cell for metal powder. Powder Metal. 38, 284–287.

Fleck, N.A., 1995. On the cold compaction of powders. J. Mech. Phys. Solids 43, 1409–1431.

Fleck, N.A., Kuhn, L.T., McMeeking, R.M., 1992. Yielding of metal powder bounded by isolated contacts. J. Mech. Phys. Solids 40, 1139–1162.

Gu, C., Kim, M., Anand, L., 2001. Constitutive equations for metal powders: application to powder forming processes. Int. J. Plast. 17, 147–209.

Gurson, A.L., 1977. Continuum theory of ductile rupture by void nucleation and growth: Part I. Yield criteria and flow rules for porous ductile media. J. Eng. Mater. Tech., Trans. ASME 99, 2–15.

Haggblad, H.A., Oldenburg, M., 1994. Modeling and simulation of metal powder die pressing with use of explicit time integration. Model. Simul. Mater. Sci. Eng. 2, 893–911.

Hofstetter, G., Simo, J.C., Taylor, R.L., 1993. A modified cap model: closest point solution algorithms. Comp. Struct. 46, 203–214.

Ji, H., Chopp, D., Dolbow, J.E., 2002. A hybrid extended finite element/level set method for modeling phase transformations. Int. J. Numer. Methods Eng. 54, 1209–1233.

Khoei, A.R., 2005. Computational Plasticity in Powder Forming Processes. Elsevier.

Khoei, A.R., Bakhshiani, A., 2004. A hypoelasto-plastic finite strain simulation of powder compaction processes with density dependent endochronic model. Int. J. Solids Struct. 41, 6081–6110.

Khoei, A.R., Lewis, R.W., 1998. Finite element simulation for dynamic large elasto-plastic deformation in metal powder forming. Finite Elem. Anal. Des. 30, 335–352.

Khoei, A.R., Lewis, R.W., 1999. Adaptive finite element remeshing in a large deformation analysis of metal powder forming. Int. J. Numer. Methods Eng. 45, 801–820.

Khoei, A.R., Nikbakht, M., 2005. Contact friction modeling with the extended finite element method, Comput. Mech., in press.

Khoei, A.R., Bakhshiani, A., Mofid, M., 2003. An endochronic plasticity model for finite strain deformation of powder forming processes. Finite Elem. Anal. Des. 40, 187–211.

Khoei, A.R., Azami, A.R., Haeri, S.M., 2004. Implementation of plasticity based models in dynamic analysis of earth and rockfill dams; a comparison of Pastor–Zienkiewicz and cap models. Comput. Geotech. 31, 385–410.

Kim, K.T., Cho, J.H., 2001. A densification model for mixed metal powder under cold compaction. Int. J. Mech. Sci. 43, 2929–2946.

Ladeveze, P., 1998. Nonlinear Computational Structural Mechanics. Springer, New York.

Lewis, R.W., Khoei, A.R., 1998. Numerical modeling of large deformation in metal powder forming. Comput. Methods Appl. Mech. Eng. 159, 291–328.

Lewis, R.W., Khoei, A.R., 2001. A plasticity model for metal powder forming processes. Int. J. Plast. 17, 1659–1692.
Lewis, R.W., Jinka, A.G.K., Gethin, D.T., 1993. Computer aided simulation of metal powder die compaction process. Powder Metall. Int. 25, 287–293.
McMeeking, R.M., Jefferson, G., Haritos, G.K., 2001. Elastic and viscoelastic response of finite particle junctions in granular materials. In: Zavaliangos, Laptev (Eds.), Recent Development in Computer Modeling of Powder Metallurgy Process. IOS Press.
Melenk, J.M., Babuska, I., 1996. The partition of unity finite element method: basic theory and applications. Comput. Methods Appl. Mech. Eng. 139, 289–314.
Moes, N., Belytschko, T., 2002. Extended finite element method for cohesive crack growth. Eng. Fract. Mech. 69, 813–833.
Moes, N., Dolbow, J.E., Belytschko, T., 1999. A finite element method for crack growth without remeshing. Int. J. Numer. Methods Eng. 46, 131–150.
Nelson, I., Baladi, G.Y., 1977. Outrunning ground shock computed with different models. J. Eng. Mech. Div., ASCE 103, 377–393.
Patzák, B., Jirásek, M., 2003. Process zone resolution by extended finite elements. Eng. Fract. Mech. 70, 957–977.
Perez-Foguet, A., Rodriguez-Ferran, A., Huerta, A., 2001. Consistent tangent matrices for density-dependent finite plasticity models. Int. J. Numer. Anal. Methods Geomech. 25, 1045–1075.
Ransing, R.S., Gethin, D.T., Khoei, A.R., Mosbah, P., Lewis, R.W., 2000. Powder compaction modelling via the discrete and finite element method. J. Mater. Des. 21, 263–269.
Redanz, P., 2001. A study of stresses in powder compacted components during and after ejection. Int. J. Solids Struct. 38, 759–775.
Sandler, I.S., Baron, M.L., 1979. Recent developments in the constitutive modeling of geological materials. In: 3rd Int. Conf. Numerical Methods in Geomechanics. A.A. Balkema, pp. 363–376.
Sandler, I.S., Rubin, D., 1979. An algorithm and a modular subroutine for the cap model. Int. J. Numer. Anal. Methods Geomech. 3, 173–186.
Sethian, J.A., 1996. A marching level set method for monotonically advancing fronts. Proc. Nat. Acad. Sci. 93, 1591–1595.
Sethian, J.A., 1999. Level Set Methods and Fast Marching Methods: Evolving Interfaces in Computational Geometry, Fluid Mechanics, Computer Vision, and Material Science. Cambridge University Press.
Shima, S., Oyane, M., 1976. Plasticity theory for porous metals. Int. J. Mech. Sci. 18, 285–291.
Simo, J.C., Ju, J.W., Pister, K.S., Taylor, R.L., 1988. An assessment of the cap model: consistent return algorithms and rate-dependent extensions. J. Eng. Mech. Div., ASCE 114, 191–218.
Stolarska, M., Chopp, D.L., Moes, N., Belytschko, T., 2001. Modeling crack growth by level sets in the extended finite element method. Int. J. Numer. Methods Eng. 51, 943–960.
Storakers, B., Fleck, N.A., McMeeking, R.M., 1999. The viscoplastic compaction of composite powders. J. Mech. Phys. Solids 47, 785–815.
Sukumar, N., Prevost, J.-H., 2003. Modeling quasi-static crack growth with the extended finite element method. Part I: Computer implementation. Int. J. Solids Struct. 40, 7513–7537.
Sukumar, N., Chopp, D.L., Moran, B., 2003. Extended finite element method and fast marching method for three-dimensional fatigue crack propagation. Eng. Fract. Mech. 70, 29–48.
Sukumar, N., Moes, N., Moran, B., Belytschko, T., 2000. Extended finite element method for three dimensional crack modeling. Int. J. Numer. Methods Eng. 48, 1549–1570.
Watson, T.J., Wert, J.A., 1993. On the development of constitutive relations for metallic powders. Metall. Trans. 24, 1993–2071.